J. Fluid Mech. (2007), *vol.* 581, *pp.* 221–250.
doi:10.1017/S0022112007005629 Printed in the United Kingdom

Torque scaling in turbulent Taylor–Couette flow between independently rotating cylinders

BRUNO ECKHARDT[1], SIEGFRIED GROSSMANN[1] AND DETLEF LOHSE[2]

[1]Fachbereich Physik, Philipps-Universität Marburg, Renthof 6, D-35032 Marburg, Germany
bruno.eckhardt@physik.uni-marburg.de; grossmann@physik.uni-marburg.de

[2]Department of Applied Physics, University of Twente, 7500 AE Enschede, The Netherlands
lohse@tnw.utwente.nl

(Received 5 July 2006 and in revised form 21 December 2006)

Turbulent Taylor–Couette flow with arbitrary rotation frequencies ω_1, ω_2 of the two coaxial cylinders with radii $r_1 < r_2$ is analysed theoretically. The current J^ω of the angular velocity $\omega(\boldsymbol{x}, t) = u_\varphi(r, \varphi, z, t)/r$ across the cylinder gap and and the excess energy dissipation rate ε_w due to the turbulent, convective fluctuations (the 'wind') are derived and their dependence on the control parameters analysed. The very close correspondence of Taylor–Couette flow with thermal Rayleigh–Bénard convection is elaborated, using these basic quantities and the exact relations among them to calculate the torque as a function of the rotation frequencies and the radius ratio $\eta = r_1/r_2$ or the gap width $d = r_2 - r_1$ between the cylinders. A quantity σ corresponding to the Prandtl number in Rayleigh–Bénard flow can be introduced, $\sigma = ((1+\eta)/2)/\sqrt{\eta})^4$. In Taylor–Couette flow it characterizes the geometry, instead of material properties of the liquid as in Rayleigh–Bénard flow. The analogue of the Rayleigh number is the Taylor number, defined as $Ta \propto (\omega_1 - \omega_2)^2$ times a specific geometrical factor. The experimental data show no pure power law, but the exponent α of the torque versus the rotation frequency ω_1 depends on the driving frequency ω_1. An explanation for the physical origin of the ω_1-dependence of the measured local power-law exponents $\alpha(\omega_1)$ is put forward. Also, the dependence of the torque on the gap width η is discussed and, in particular its strong increase for $\eta \to 1$.

1. Introduction

Taylor–Couette (TC) flow in the gap between two independently rotating coaxial cylinders supports molecular and convective transfer of azimuthal momentum between these cylinders. This leads to a net loss of angular momentum of one of the externally driven cylinders, which can be measured as a torque T, cf. Lathrop, Fineberg & Swinney (1992*a*,*b*), Lewis & Swinney (1999). Its dependence on the rotation frequencies of the cylinders is of interest for understanding the gross features of the flow.

Measurements of the torque T, either in units Nm or in dimensionless form $G = T/(2\pi\ell\rho_{fluid}\,\nu^2)$ have been described not only by Lathrop *et al.* (1992*a*,*b*) and Lewis & Swinney (1999) but also by Wendt (1933), Taylor (1936*a*, *b*), Tong *et al.* (1990), and Lim & Tan (2004). Here, ℓ is the length of the cylinders, ρ_{fluid} the mass density of the fluid, and ν its kinematic viscosity. The scaling exponent α, defined by $G \propto R_1^\alpha$ for the dimensionless torque G as a function of the inner cylinder rotation

Reynolds number $R_1 = r_1\omega_1 d/\nu$, has most recently been reported by Lewis & Swinney (1999). Its value turned out to depend on R_1 and range from about $\alpha = 1.6$ to $\alpha = 1.8$ if R_1 varies from 10^4 to 10^6. Thus $\alpha(R_1)$ is in fact a local exponent. There is no global power-law behaviour. Wendt (1933) fitted $\alpha = 1.5$ for $4 \times 10^2 < R_1 < 10^4$ and $\alpha = 1.7$ in the range $10^4 < R_1 < 10^5$, i.e. he measured an increasing exponent with increasing rotation rate R_1. He furthermore measured a non-trivial dependence of G on the radius ratio $\eta = r_1/r_2$ and on the non-dimensional gap width $1 - \eta$ in both the small and medium gap ranges, which he fitted as $G \propto \eta^{3/2}(1-\eta)^{-7/4}$. Tong *et al.* (1990) measured the torque in a TC system having an even larger gap, with $\eta = 0.448$. Lathrop (1992) gave the radius ratio dependence $\eta^{5/3}(1-\eta)^{-5/3}$, extending a prediction by Marcus (1984*a*, *b*) for $\eta \to 1$. Lathrop *et al.* (1992*b*) discussed an infinite-Reynolds-number argument leading to $G \propto \eta(1+\eta)(1-\eta)^{-2}R_1^2$, i.e. $\alpha = 2$. This value of α was also advocated by Nickerson (1969) and by Doering & Constantin (1992) (here as an upper bound).

The purpose of this work is to address the physical origin of the Reynolds number R_1 dependence of the scaling exponent $\alpha(R_1)$. Previously, this dependence has been parameterized by fitting to a logarithmic law in analogy to pipe flow resistance. The main argument for its validity is a self-similar flow structure. But doubts remain on whether this holds for the range of Reynolds numbers R_1 reached in these experiments, which are not asymptotically large. In particular, the boundary layers are not yet turbulent. We study here another possible origin of the R_1-dependence of α, which has been successfully applied to understand the observed variation of scaling in thermal Rayleigh–Bénard (RB) convection. The idea is that $\alpha(R_1)$ varies with R_1 because of the varying contributions made by the bulk and the boundary layers to the angular momentum current and to the dissipation rate. Our analysis follows the same arguments as used for RB flow. Comparison of our calculated $\alpha(R_1)$ with experiment turns out to be quite promising.

TC flow has long been known to have a similarity to RB flow, which is driven by a temperature difference between a bottom and a top plate in the gravity field of the Earth. The relevant physical quantity being transported in RB convection is thermal energy (heat) instead of angular momentum. The non-dimensionalized heat flux is the Nusselt number *Nu*. The analogy between RB and TC flow was first developed in Bradshaw (1969). Next it was used by Eckhardt, Grossmann & Lohse (2000) to analyse the torque in TC flow and the friction factor in pipe flow along the lines developed in Grossmann & Lohse (2000) for RB flow. Dubrulle & Hersant (2002) used the RB–TC analogy to introduce a one-to-one mapping of corresponding field components (most easily done in restricted geometries, see Eckhardt, Grossmann & Lohse 2005) and to derive the scaling behaviour of the torque in TC flow in analogy to that of the heat transport in RB flow, with a modelling idea different from the one proposed here. Also, the work of van den Berg *et al.* (2003) should be mentioned in this context.

In the following we propose a new form of the RB–TC analogy. It is based on a global relation between the turbulent convective dissipation rate ε_w and the relevant transport current J^ω together with a Navier–Stokes-based definition of J^ω in terms of correlations. The second part of this novel idea is to introduce the existence of a wind Reynolds number R_w in addition to the externally controlled rotation Reynolds numbers of the cylinders to model J^ω and ε_w and their exact relations in terms of R_w. The wind has already been introduced to derive the scaling of the heat flux *Nu* in RB flow and also the torque scaling in TC flow, cf. Grossmann & Lohse (2000) and Eckhardt *et al.* (2000). It was studied further in Eckhardt *et al.* (2005). The present

approach generalizes this idea systematically to derive new scaling behaviour of the torque in TC flow, leading to a variable exponent $\alpha(R_1)$. The correspondence between TC and RB flow can be extended to pipe flow (Eckhardt, Grossmann & Lohse 2007), for which the radial transport of axial velocity leads to skin friction and thus to a resistance for the mass flow through the pipe.

In RB flow one measures or calculates the heat current Q or thermal current $J^\theta = Q/c_p\rho_{fluid}$. Its non-dimensional form is the Nusselt number $Nu = Q/(\Lambda\Delta L^{-1}) = J^\theta/(\kappa\Delta L^{-1})$. The heat is convected through a container, filled with fluid with Prandtl number $Pr = \nu/\kappa$ under varying external driving, described by the Rayleigh number $Ra = \alpha_p g L^3\Delta/\nu\kappa$. Here, c_p is the specific heat, Λ the heat conductivity, Δ the temperature difference between bottom and top plate, L the height of the RB cell, α_p the isobaric thermal expansion coefficient, g the Earth's gravitional acceleration. Again, ν denotes the kinematic viscosity of the fluid and $\kappa = \Lambda/(c_p\rho_{fluid})$ its thermal diffusivity. Incompressibility and the Boussinesq–Oberbeck approximation are assumed to be valid. To determine Nu the basic idea is to analyse the kinetic and the thermal dissipation rates ε_u, ε_θ of the turbulent flow in the RB container (Grossmann & Lohse 2000, 2001, 2002; Grossmann & Lohse 2004). These rates are decomposed into contributions with different scaling behaviour. The relevant decomposition for the velocity dissipation rate ε_u consists of distinguishing the boundary layer and the bulk contributions. The thermal dissipation rate ε_θ on the other hand cannot be decomposed into its boundary and bulk parts. Instead, it is partitioned according to contributions with different scaling behaviour (Grossmann & Lohse 2004). The relevant parts are (i) the boundary layers together with the detached boundary layer or plume contributions in the bulk and (ii) the background fluctuations, both in the bulk and near the boundaries. These two parts scale differently with Ra and Pr. Because of a close connection between the thermal dissipation rate ε_θ and the heat current Nu – in fact, these two quantities are equal except for dimensional factors – one can alternatively decompose the heat current $J^\theta = \kappa\Delta L^{-1} Nu$ into contributions with different scaling behaviour, as was analysed in Grossmann & Lohse (2004).

In case of TC flow there are also two relevant fields, which correspond to the velocity $\boldsymbol{u}$ and the temperature θ in RB convection. Instead of the three-dimensional velocity field $\boldsymbol{u}$ in RB convection we have the two-dimensional transverse velocity field $\boldsymbol{u}_\perp = (u_r, u_z)$ in TC flow. Instead of the temperature profile between the bottom and top plates in RB, in the TC geometry there is a radial profile of the angular velocity $\omega(r)$ between the angular velocities ω_1, ω_2 of the independently rotating cylinders. In both cases, RB as well as TC, all four or three field components are coupled by the equations of motion, also four or three of them. A direct relation between field components is possible when RB flow is restricted to a plane, see Eckhardt *et al.* (2005).

The angular velocity profile can also be understood as an azimuthal velocity profile $u_\varphi = r\omega(r)$ or an angular momentum profile $L(r) = ru_\varphi = r^2\omega(r)$. This profile gives rise to a current J^ω of ω (or of u_φ or L), which corresponds to the thermal current J^θ in RB flow. It will turn out that the transport current J^ω is a non-trivial, interesting quantity. The superscript ω on J^ω indicates that the current characterizes the transport of the angular velocity field $\omega(\boldsymbol{x}, t)$ rather than of the velocity component u_φ or of the angular momentum L fields, although intuitively one might have expected L- or u_φ-transport instead of ω-transport; of course, all these are closely related.

For a larger difference $\omega_1 - \omega_2$ there is, in addition to the molecular transport of ω, also a convective transport. This is provided by the radial velocity component u_r that is accompanied by u_z. Both components u_r and u_z are coupled to u_φ via the

Navier–Stokes and continuity equations. It is the *additional* energy dissipation rate due to this radial convection, called ε_w, which is relevant for the convective ω-transport. We define it as $\varepsilon_w = \varepsilon - \varepsilon_{lam}$, where ε is the total energy dissipation rate per unit mass of the full velocity field and ε_{lam} the energy loss already present in the laminar state. ε_{lam} is subtracted because it does not contribute to the convective radial transport.

The basic equations will be the exact relation between ε_w and J^ω on the one hand and the dependence on both angular velocities ω_1, ω_2 of the cylinders as well as on the radius ratio η or gap width $1-\eta$ on the other hand. The frequencies ω_i and the radius ratio η are the external control parameters. The orthogonal components u_r, u_z of the flow field are fluctuating or manifested as a large-scale coherent flow, in either case denoted as the 'wind'. We characterize the magnitude of the wind by its amplitude U, or by the corresponding wind Reynolds number $R_w = Ud/\nu$, as in Eckhardt *et al.* (2000, 2005). Note that U and R_w, as the response of the fluid, are not yet determined. In particular, they need not coincide with other characteristic velocities of the system, such as the velocities of the cylinders. R_w corresponds to $Re = UL/\nu$ in RB flow, see Grossmann & Lohse (2000, 2001, 2002); Grossmann & Lohse (2004). Hairpin vortices are considered as the isothermal analogue of the thermal plumes, detaching from the boundary layers of the container. In RB flow the plumes seem to be more sheet-like for small and medium Prandtl numbers, but mushroom-like for larger ones, cf. Breuer *et al.* (2004) and Funfschilling & Ahlers (2004). It needs further experiments to clarify if a similar structural change of the hairpins from two- to one-dimensional structures occurs as the gap width is varied. Furthermore, one can introduce a parameter $\sigma = \sigma(\eta)$, depending on the radius ratio η or gap width $1-\eta$, i.e. on the geometry of the TC apparatus; σ will play a role analogous to the Prandtl number Pr in RB convection as will be discussed in §§3.1 and 5. The η-dependence has been experimentally explored only in part. We shall see that our results can be compared with Wendt's (1933) data. The case of counter-rotation of the confining cylinders is non-trivial. Here, the role of the neutral surface still has to be analysed. It divides the flow volume into the physically rather different inner and outer parts of the gap. We shall not address this case in full generality and detail.

We start by defining the relevant geometric parameters of the experiment and the equations of the velocity field in cylindrical coordinates (§2), and then consider in §3 the proper definition of the angular velocity current J^ω and its non-dimensionalized form N^ω (corresponding to J^θ and the Nusselt number Nu in RB flow). In §4 we calculate the dissipation rate ε_w in terms of the control parameters ω_1, ω_2, and the current J^ω. Based on these quantities we derive model equations for N^ω and the transverse velocity amplitude U or R_w in §5. Their solution determines the scaling behaviour of the wind Reynolds number R_w and of the torque G. The latter can be successfully compared with existing data, §6. We close with conclusions in §7.

2. Equations of motion

Consider two concentric cylinders which can rotate around their common axis, the gap between them being filled with an incompressible fluid with kinematic viscosity ν and mass density ρ_{fluid}. In the following, the joint cylinder axis is chosen as the z-axis of the cylindrical coordinate system used; r and φ denote its radial and azimuthal coordinates. The inner and outer cylinder radii are $r = r_1$ and $r = r_2$, and $d = r_2 - r_1$ is the gap width. The control parameters are the angular velocities ω_1 and ω_2 of the inner and outer cylinders or the corresponding Reynolds numbers $R_i = r_i \omega_i d/\nu$, $i = 1, 2$. We take $\omega_1 > 0$ by definition, and ω_2 can be positive (co-rotating case)

or negative (counter-rotating case). The no-slip boundary condition means that the velocities of the fluid at the cylinder surfaces are $v_1 = r_1\omega_1$ (inner) and $v_2 = r_2\omega_2$ (outer). The arithmetic mean radius is defined as $r_a = (r_1 + r_2)/2$, the geometric mean radius as $r_g = \sqrt{r_1 r_2}$, and the radius ratio as $\eta = r_1/r_2$, with $0 < \eta < 1$. The angular momenta at the cylinder surfaces are $L_1 = r_1 v_1 = r_1^2\omega_1$ and L_2 correspondingly. The angular velocity difference $\omega_1 - \omega_2$ may be positive or negative, and the same holds for the Reynolds number difference $R_1 - R_2$. Our theory deals with the ideal case of infinite aspect ratio $\Gamma = \ell/d$, i.e. infinitely long cylinders $\ell \to \infty$. In practice, Γ is of order 10. Typical values in Lewis & Swinney (1999) are $r_1 = 16\,\mathrm{cm}$, $r_2 = 22.09\,\mathrm{cm}$, $d = 6.09\,\mathrm{cm}$, $r_a = 19.05\,\mathrm{cm}$, $r_g = 18.80\,\mathrm{cm}$, $\eta = 0.724$, $\ell = 69.5\,\mathrm{cm}$, $\Gamma = 11.4$; the viscosity ν ranges from $0.968\,\mathrm{mm^2\,s^{-1}}$ for water to $20.8\,\mathrm{mm^2\,s^{-1}}$ for a glycerol–water mixture.

The laminar flow between the independently rotating cylinders has an azimuthal component $u_\varphi = v_{lam}(r)$ only, independent of φ and z. The other two velocity components u_r, u_z are zero. The laminar profile is

$$v_{lam}(r) = Ar + B/r, \qquad A = \frac{\omega_2 - \eta^2\omega_1}{1-\eta^2}, \qquad B = \frac{(\omega_1 - \omega_2)r_1^2}{1-\eta^2}. \tag{2.1}$$

The units are $[A] = [\omega] = \mathrm{s^{-1}}$ and $[B] = [\omega r^2] = \mathrm{m^2\,s^{-1}} = [\nu] = [L]$.

In general TC flow, beyond laminarity, the velocity field $\boldsymbol{u}(r, \varphi, z)$ has three components: the longitudinal one $u_\varphi = v$ and two perpendicular ones $(u_r, u_z)^+ = \boldsymbol{u}_\perp$. All components depend on all variables r, φ, and z. The equations of motion are the Navier–Stokes equations for incompressible fluid flow in cylindrical coordinates (see e.g. Landau & Lifshitz 1987),

$$\partial_t u_r = -(\boldsymbol{u}\cdot\nabla)u_r + \frac{u_\varphi^2}{r} - \partial_r p + \nu\left(\Delta u_r - \frac{u_r}{r^2} - \frac{2}{r^2}\partial_\varphi u_\varphi\right), \tag{2.2}$$

$$\partial_t u_\varphi = -(\boldsymbol{u}\cdot\nabla)u_\varphi - \frac{u_r u_\varphi}{r} - \frac{1}{r}\partial_\varphi p + \nu\left(\Delta u_\varphi - \frac{u_\varphi}{r^2} + \frac{2}{r^2}\partial_\varphi u_r\right), \tag{2.3}$$

$$\partial_t u_z = -(\boldsymbol{u}\cdot\nabla)u_z - \partial_z p + \nu\Delta u_z. \tag{2.4}$$

The differential operators in these equations have the following meaning:

$$(\boldsymbol{u}\cdot\nabla)\, f = \left(u_r\partial_r + u_\varphi\frac{1}{r}\partial_\varphi + u_z\partial_z\right) f, \tag{2.5}$$

and

$$\Delta f = \frac{1}{r}\partial_r(r\partial_r f) + \frac{1}{r^2}\partial_\varphi^2 f + \partial_z^2 f. \tag{2.6}$$

Note that p is the kinematic pressure; the physical pressure is $\rho_{fluid} \times p$. The continuity equation in cylindrical coordinates is

$$\frac{1}{r}\partial_r(r u_r) + \frac{1}{r}\partial_\varphi u_\varphi + \partial_z u_z = 0. \tag{2.7}$$

The boundary conditions have already been described: $\boldsymbol{u}_\perp = 0$ and $u_\varphi(r_i) = v_i = r_i\omega_i$, $i = 1, 2$, at the cylinder surfaces.

The whole set of coupled equations will be considered, including the φ-dependence of the fields. No simplification such as $\partial_\varphi \approx 0$ is used nor allowed in the turbulent case.

3. Angular momentum current

3.1. *Definition*

If the rotation velocities of the cylinders are different, $\omega_1 \neq \omega_2$, there is an r-dependent profile of the azimuthal velocity u_φ and corresponding profiles of the angular velocity ω and of the angular momentum L. The consequence is a molecular as well as a convective transport of azimuthal momentum. To derive the corresponding u_φ-current, we average the u_φ- or v-equation (2.3) over a cylindrical surface of height ℓ and area $A(r) = 2\pi r\ell$, chosen to be co-axial to the rotating TC cylinders and lying between them, $r_1 \leqslant r \leqslant r_2$. (For convenience we shall also use the notation v for the longitudinal component u_φ.) Note that this $A(r)$-average commutates with functions of r, because it is r-independent,

$$\langle \ldots \rangle_A = \int \frac{r\,\mathrm{d}\varphi\,\mathrm{d}z}{2\pi r\ell} \ldots = \int \frac{\mathrm{d}z}{\ell} \int \frac{\mathrm{d}\varphi}{2\pi} \ldots .$$

We also time average (2.3) and find

$$0 = \left\langle -u_r\partial_r v - u_z\partial_z v - \frac{u_r v}{r} + \nu\left(\frac{1}{r}\partial_r(r\partial_r v) - \frac{v}{r^2}\right)\right\rangle_{A,t}. \tag{3.1}$$

Using the continuity equation $\partial_z u_z = -(1/r)\partial_r(ru_r) - (1/r)\partial_\varphi v$ we have

$$0 = \left\langle -u_r\partial_r v - v\partial_r u_r - \frac{2vu_r}{r} + \nu\left(\frac{1}{r}\partial_r r\partial_r v - \frac{v}{r^2}\right)\right\rangle_{A,t}. \tag{3.2}$$

The first three terms sum to $r^{-2}\partial_r(r^2 u_r v)$. After multiplication with r^2 (which commutes with $\langle \ldots \rangle_A$) and also writing the viscous term as an r-derivative one obtains

$$0 = \partial_r(r^3[\langle u_r\omega\rangle_{A,t} - \nu\partial_r\langle\omega\rangle_{A,t}]). \tag{3.3}$$

The conclusion is that the quantity $r^3[\ldots]$, must be independent of r, i.e. it has the same value for any $A(r)$-surface for all r with $r_1 \leqslant r \leqslant r_2$. In any event, it does not depend on t, φ, or z because of the averaging on these variables. We consequently interpret the constant

$$J^\omega = r^3[\langle u_r\omega\rangle_{A,t} - \nu\partial_r\langle\omega\rangle_{A,t}] \tag{3.4}$$

as the conserved transverse current of azimuthal motion (possibly up to a constant factor), transporting $\omega(\boldsymbol{x}, t)$ in the radial direction. Its unit is $[J^\omega] = \mathrm{m}^4\,\mathrm{s}^{-2} = [L]^2 = [\nu]^2$.

The essential elements in (3.4) are contained in the angular brackets $\langle \ldots \rangle$. The first such term reflects a 'Reynolds stress' and the second one a viscous derivative of a mean profile. This contribution occurs only with $\omega(r)$ for the mean profile but not with $L(r)$, as our derivation from the Navier–Stokes equation has shown. The Reynolds stress itself could also be expressed as $\langle L^2\rangle$, but the viscous derivative is not $\nu\partial_r\langle L\rangle$ but instead $\nu\partial_r\langle\omega\rangle$. It is this property which distinguishes the ω-field from the L-field.

The dimensionless expression $\nu^{-2}J^\omega$ is equal to the non-dimensionalized expression G for the torque T, which has been introduced above in § 1, namely $T = 2\pi\ell\rho_{fluid}\,\nu^2 G = 2\pi\ell\rho_{fluid}J^\omega$, i.e. $G = \nu^{-2}J^\omega$. To see this, consider the r,φ-component $\sigma_{r\varphi}$ of the stress tensor (cf. Landau & Lifshitz 1987) at the inner cylinder $r = r_1$,

$$\sigma_{r\varphi}(r_1) = -\eta_{viscosity}\left(\frac{\partial u_\varphi}{\partial r} - \frac{u_\varphi}{r}\right)_{r_1} = -\rho_{fluid}\;\nu\;r_1\left(\frac{\partial\omega}{\partial r}\right)_{r_1} = \rho_{fluid}\;r_1^{-2}J^\omega. \tag{3.5}$$

Multiplying by the surface area $2\pi r_1 \ell$ gives the force on the inner cylinder and another factor of r_1 leads to the torque, thus $T = 2\pi\ell\rho_{fluid} J^{\omega}$.

The expression (3.4) is close to that discussed in an appendix to Smith & Townsend (1982). The particular form of J^{ω} according to the definition (3.4) indicates that the proper field which has to be considered as the transported quantity is ω, and neither the azimuthal velocity $v = u_{\varphi} = r\omega$ nor the angular momentum $L = r^2\omega$. Namely, it is the $\langle\omega\rangle_{A,t}$-slope, which describes the molecular transport. Of course, one can express ω in (3.4) as L/r^2, but r^{-2} does not commute with ∂_r. It is just the expression (3.4) which is the analogue of the heat current

$$J^{\theta} = \langle u_3\theta\rangle_{A,t} - \kappa\partial_z\langle\theta\rangle_{A,t} \tag{3.6}$$

in thermally driven RB flow. Consequently, it is ω which plays the role corresponding to the temperature θ. Still, J^{ω} contains an additional factor of r^3 besides the A-cylinder averages. This factor of r^3 is non-trivial. Mathematically, it means that because it does not commute with ∂_r in (3.4), the remaining factor [...] is not r-independent; r enters [...] as the radius of the respective $A(r)$-cylinders.

Physically, the factor r^3 implies that the outer flow ranges are more dominant than the inner ones. This corresponds to the observation that the inner range is more vivid and active in forming structures than the outer one, which seems less filled with structures. But inner and outer parts must contribute to the transverse transport of the azimuthal velocity with the same magnitude. This requires the enhancement which is provided by the explicit factor r^3 in the ω-current J^{ω}.

Despite of these arguments one might ask if the equations of motion also allow an L-current to be defined. The idea is that instead of averaging the u_{φ}-equation (2.3) it would be better to consider the corresponding L-equation. This might be obtained by taking r times the u_{φ}-equation. But proceeding with this as before and respecting that r commutes with the $A(r)$-average, one ends up with the same equation (3.3) as before. And, incidentally, the same finding results after dividing (2.3) by r in order to analyse an ω-equation of motion from the beginning. These observations support the interpretation of J^{ω} according to (3.4) as the relevant current and identifying the angular velocity field $\omega(\boldsymbol{x}, t)$ as the transported physical quantity, for it is the $\langle\omega\rangle_{A,t}(r)$ profile whose r dependence is relevant. Of course, the convective term in J^{ω} can be written as $r\langle u_r L\rangle_{A,t}$ so that it becomes, still up to an additional factor of r, the time- and area-averaged correlation between the transverse velocity u_r and the angular momentum L.

As an immediate consequence of this discussion, for any r with $r_1 \leqslant r \leqslant r_2$ we can write

$$\langle u_r\omega\rangle_{A(r),t} - \nu\partial_r\langle\omega\rangle_{A(r),t} = J^{\omega}\, r^{-3}. \tag{3.7}$$

The sum of the (u_r, ω)-correlation and the viscous ω-gradient decreases in the gap $\propto 1/r^3$. The factor of proportionality is the r-independent ω-current J^{ω}. Equation (3.7) gives a means of measuring J^{ω} in the interior of the flow. It is valid without any approximation or model assumption. It holds for arbitrary gap width, small as well as large, and for co- as well as counter-rotating cylinders. Equation (3.7) is an exact relation whose validity can be used as an experimental check.

Another noteworthy consequence of the J^{ω}-definition is that the ratio of the ω-slopes at the outer and inner cylinders strongly decreases with decreasing radius ratio η or increasing gap width $1 - \eta$. From (3.4) taken at $r = r_1$ and $r = r_2$ one obtains

$$\partial_r\langle\omega\rangle\,|_{r_2} = \eta^3\partial_r\langle\omega\rangle\,|_{r_1}\,. \tag{3.8}$$

This indicates a significant difference between the $\langle\omega\rangle_{A,t}$ profile near the inner cylinder and that near the outer one. In particular, if one defines the ω-field boundary layer thicknesses $\lambda_{1,2}$ at the cylinders by

$$\partial_r \langle\omega\rangle_{A,t} \,|_{r_i} \equiv \frac{\Delta_i}{\lambda_i}, \quad i = 1, 2, \tag{3.9}$$

introducing the ω-decrease $\Delta_i = |\, \omega_i - \bar{\omega} \,|$ between the rotation rates ω_i of cylinders i and a properly chosen distinguished bulk or centre level $\bar{\omega}$ of the $\langle\omega\rangle_{A,t}$ profile representative of the bulk of the gap, then two different boundary layer thicknesses exist due to the different initial slopes at the inner and outer cylinders. The λ_i according to the definition (3.9) are known as *slope thicknesses*, because they are based on the slopes at the surfaces; they do not express the detailed shapes of the profiles in the respective boundary layers. λ_1 and λ_2 are related by

$$\lambda_2 = \eta^{-3} \frac{\Delta_2}{\Delta_1} \lambda_1. \tag{3.10}$$

According to the factor η^{-3} the outer boundary layer thickness will usually be much larger than the inner one for smaller η or larger gap $\propto 1 - \eta$. But of course, the ratio Δ_2/Δ_1 will also vary with η and probably become smaller.

In the small-gap limit, $d \to 0$ or $\eta \to 1$, the factor r^3 in J^ω is, to a good approximation, equal to r_a^3 or r_g^3. In small-gap systems, which are similar to channel flow, there is no particular enhancement of the outer relative to the inner range. For small-gap systems the flux J^ω then has the same structure as J^θ in RB flow, except for the now nearly constant prefactor. In TC systems with broader gap the definition (3.4) guarantees that J^ω stays constant when r is varied between the cylinder radii r_1 and r_2, i.e. (3.4) is the correct formula for the current J^ω transverse to the angular motion.

In laminar TC flow there is no u_r-component. Then only the second, molecular transport term in J^ω, the r-derivative, contributes. Inserting $\omega(r) = A + B/r^2$ from (2.1) into (3.4) one obtains

$$J^\omega_{lam} = 2\nu B = 2\nu r_1^2 r_2^2 \frac{\omega_1 - \omega_2}{r_2^2 - r_1^2}. \tag{3.11}$$

It is the externally controlled ω-difference at the cylinders that drives the ω-flux. If the inner cylinder revolves faster, we have $J^\omega > 0$, i.e. azimuthal momentum is flowing from the inner to the outer cylinder. In particular this is always so for counter-rotating cylinders. For an inner cylinder at rest or generally for $\omega_2 > \omega_1$ we observe a transport of azimuthal momentum from the outer to the inner cylinder's surfaces.

Clearly, the laminar current J^ω_{lam} of (3.11) is not only an r-independent constant, it is also the physical analogue of $\kappa \Delta L^{-1}$, the molecular heat flux in RB cells, except for a factor $r^3 \approx r_a^3$, which takes care of the different physical dimensions of J^ω_{lam} and $\kappa \Delta L^{-1}$. One might wish to physically identify $\omega_1 - \omega_2$ with the temperature difference Δ between bottom and top, and $r_2 - r_1 = d$ with the height L of the RB container. The remaining factor $\nu r_1^2 r_2^2 / r_a$ (divided by the characteristic additional factor r_a^3) can then be understood as corresponding to the thermal diffusivity κ. By this argument a dimensionless quasi-Prandtl number, denoted as σ, arises:

$$\kappa \equiv \nu \frac{r_1^2 r_2^2}{r_a^4}, \quad \sigma \equiv \frac{\nu}{\kappa} = \frac{r_a^4}{r_g^4} = \left(\frac{(1+\eta)/2}{\sqrt{\eta}} \right)^4. \tag{3.12}$$

η	1.0	0.9	0.8	0.7	0.6	0.5	0.4	0.3	0.2	0.1
σ	1.000	1.006	1.025	1.065	1.138	1.266	1.501	1.983	3.240	9.150

TABLE 1. The geometrical quasi-Prandtl number $\sigma = (((1+\eta)/2)/\sqrt{\eta})^4$ for decreasing radius ratio $\eta = r_1/r_2$ or correspondingly increasing gap width $1-\eta$. For most TC-devices σ is near to 1 or at best 2. It is only for very broad gaps (small η) that σ grows significantly.

Both σ and κ describe geometric properties of the TC system, since they depend on its radius ratio η or gap width $1-\eta$. The factor r_a^3 has been incorporated because $J^\theta = \kappa L^{-1}\Delta$ is a velocity $\times$ transported temperature. By comparing it with J^ω_{lam}, being r^3 times velocity $\times$ transported angular velocity, the ratio J^ω_{lam}/r_a^3 is the appropriate analogue of J^θ. In the narrow-gap case $\eta \to 1$ one finds $\sigma \to 1$. For decreasing inner cylinder radius r_1 or $\eta \to 0$ and corresponding broadening of the gap, we have $\sigma \to \infty$. TC flow in the commonly used containers is thus expected to have similarity with RB flows with Prandtl numbers which are larger than but still close to $\sigma = 1$. In the apparatus of Lewis & Swinney (1999) $\sigma = 1.054$ according to the cylinder radii reported in § 2. A survey on the dependence of $\sigma(\eta)$ on η is given in table 1.

We emphasize the meaning of the quasi-Prandtl number σ and of the quasi-diffusivity κ again: In both cases, RB and TC flow, the laminar current densities J^θ_{lam} and J^ω_{lam} are proportional to the driving gradient of the relevant profile, Δ/L or $(\omega_1-\omega_2)/d$, respectively. In RB the factor of proportionality is the fluid property κ, thermal diffusivity; in TC it is a product of ν and a factor defined in terms of the radii r_1, r_2 of the TC cylinders, i.e. of purely geometric origin. By analogy this product is called the quasi-diffusivity κ, and ν divided by this κ is correspondingly called the quasi-Prandtl number σ. This quantity σ depends on r_1, r_2 and thus on the radius ratio η only, and, in contrast to Pr, is always larger than 1.

We now wish to non-dimensionalize J^ω properly in order to define a TC-analogue N^ω of the Nusselt number Nu in RB flow. We argue that in RB the fluid at rest with a temperature gradient Δ/L corresponds to the laminar TC flow, which has an ω profile due to the angular velocity difference $\omega_1-\omega_2$, but no transverse advection. This correspondence is further confirmed by noting that for increasing external driving (either by increasing the temperature difference or the angular velocity difference) the state with dissipative patterns arises, namely roll formation in both cases. We therefore non-dimensionalize the angular velocity current J^ω by dividing it with J^ω_{lam}, corresponding to dividing J^θ by $\kappa L^{-1}\Delta$ in RB flow:

$$N^\omega = \frac{J^\omega}{J^\omega_{lam}} = \frac{r^3[\langle u_r\omega\rangle_{A,t} - \nu\partial_r\langle\omega\rangle_{A,t}]}{2\nu B}. \tag{3.13}$$

The quantity N^ω measures how effective the transverse convective angular velocity transport is in terms of the purely molecular transverse transport. Note that this dimensionless quantity N^ω is different from the dimensionless torque $G = \nu^{-2}J^\omega$ as introduced and measured previously (Lathrop *et al.* 1992*a*,*b*; Lewis & Swinney 1999). They are related by

$$G = \nu^{-2}J^\omega_{lam}\,N^\omega. \tag{3.14}$$

Though G also is dimensionless, it physically compares the J^ω-transport with the purely molecular transport ν^2 in a fluid at rest, instead of comparing with the molecular transport in a laminar but not yet transversely convecting flow, namely with $J^\omega_{lam} = 2\nu B$ of (3.11). Dubrulle & Hersant (2002) also introduced the ratio

between the torques in the turbulent and the laminar states, $G/G_{lam} \equiv N$, as the relevant dimensionless quantity.

3.2. *Angular momentum conservation*

The prominent role of ω instead of L seems surprising at first sight: the angular momentum L might be expected to be a conserved quantity in TC flow and thus should play a distinguished role. The well-known Rayleigh stability criterion for the laminar state, guaranteeing stability before the onset of Taylor vortices, rests on the idea of conserved L, cf. Landau & Lifshitz (1987), or its full viscous extension in Esser & Grossmann (1996). How can one check such L-conservation from the equations of motion?

$L = ru_\varphi = rv(r, \varphi, z; t)$ is a field variable, which in turbulent flow is of course time dependent. We, therefore, consider the volume-averaged magnitude squared of the angular momentum field $\langle L^2 \rangle_V$ and its possible conservation in time. To calculate the time dependence of this quantity, we start from the v-equation (2.3), multiply it by r (to obtain an L-equation), then multiply it again by L (to obtain $\partial_t(L^2/2)$), and finally volume average.

Having this in mind we first multiply (2.3) by v and rearrange the $(v^2/2)$-equation to obtain

$$\partial_t \frac{v^2}{2} = -\left[u_r \partial_r \frac{v^2}{2} + \frac{v}{r}\partial_\varphi \frac{v^2}{2} + u_z \partial_z \frac{v^2}{2} + \frac{u_r v^2}{r} + \frac{v}{r}\partial_\varphi p\right] + \nu v(\ldots). \tag{3.15}$$

This can be rearranged using again the continuity equation ($\times v^2/2$) and combining the two terms with u_r into one term with an appropriate derivative to obtain

$$\partial_t \frac{v^2}{2} = -\frac{1}{2}\left[\frac{1}{r^3}\partial_r r^3 u_r v^2 + \frac{1}{r}\partial_\varphi v^3 + \partial_z u_z v^2\right] - \frac{v}{r}\partial_\varphi p + \nu v(\ldots). \tag{3.16}$$

We now volume average, i.e. integrate with the volume elements $r\mathrm{d}r\mathrm{d}\varphi\mathrm{d}z/V$. The second and third terms in (3.16) vanish immediately under φ- and z-integration. The first term however only vanishes after the additional multiplication with r^2; it does so because $u_r = 0$ at $r = r_1, r_2$. Thus, the product of r and u_φ to form L^2 is uniquely singled out in that the bracket contributions [...] vanish after averaging. For ideal, inviscid TC fluid flow we then have

$$\partial_t \left\langle \frac{L^2}{2} \right\rangle_V = -\langle L \partial_\varphi p \rangle_V. \tag{3.17}$$

In laminar TC flow the kinematic pressure p is independent of φ, which leads to angular momentum conservation $\langle L^2 \rangle_V = \text{const}$ in laminar TC flow. This reconfirmes the validity of Rayleigh's, Landau's, etc. argument for the stability boundary of laminar TC flow. If, instead, the flow is turbulent, there will also be pressure fluctuations in φ-direction. These lead to a coupling of the L-motion to the other degrees of freedom. Note incidentally that φ is the canonical conjugate variable to L.

Of course, viscosity in both the laminar and turbulent case is a sink of angular momentum,

$$\partial_t \left\langle \frac{L^2}{2} \right\rangle_V = -\langle L \partial_\varphi p \rangle_V + \nu \langle r^2 v \Delta v - v^2 + 2v\partial_\varphi u_r \rangle_V. \tag{3.18}$$

The last term, describing the viscous loss, can be rearranged to describe angular momentum loss by negative definite terms, by v-energy, and by coupling to the wind

$\propto u_r$. In addition, there are boundary contributions:

$$\text{viscous loss} = -\nu\langle(\partial_\varphi v)^2 + r^2(\partial_z v)^2 + v^2 + 2u_r\partial_\varphi v - rv\partial_r r\partial_r v\rangle_V. \tag{3.19}$$

We do not discuss this expression here, but consider instead the total energy dissipation rate in the following section.

4. Energy dissipation rate

Let us now calculate the energy balance in TC flow. Expressions for the dissipation rate per mass in TC systems are available in the literature, e.g. Lewis & Swinney (1999) use

$$\begin{aligned}\langle\varepsilon\rangle &= \frac{\text{viscous force}\times\text{velocity}}{\text{mass}} = \frac{\text{torque}\times\text{angular velocity}}{\text{mass}} \\ &= \frac{T\ \omega_1}{2\pi(r_2^2-r_1^2)\ell\rho_{fluid}} = \frac{J^\omega\ \omega_1}{(r_2^2-r_1^2)}.\end{aligned} \tag{4.1}$$

We shall derive the total energy dissipation rate per mass from the equations of motion. The three equations of motion (2.2), (2.3), and (2.4) are the r-, φ-, and z-components of the Navier–Stokes equations. Multiplying them by u_r, u_φ, and u_z, respectively, adding and volume averaging leads to $\langle u_r\partial_t u_r + u_\varphi\partial_t u_\varphi + u_z\partial_t u_z\rangle_V$, i.e. to the kinetic energy balance

$$\partial_t\left\langle\frac{\boldsymbol{u}^2}{2}\right\rangle_V = \langle-\boldsymbol{u}\cdot[(\boldsymbol{u}\cdot\nabla)\boldsymbol{u}] - (\boldsymbol{u}\cdot\nabla)p + \nu\boldsymbol{u}\cdot(\Delta\boldsymbol{u})\rangle_V \tag{4.2}$$

as usual. The energy balance contains a convective surface term, which does not contribute, since $\mathrm{d}\boldsymbol{A}\cdot\boldsymbol{u} = 0$ at the boundary. (Note that the vector $\boldsymbol{u}$ itself does not vanish at the surface. It has a non-vanishing component, namely $u_\varphi(= v)$. Only $\boldsymbol{u}_\perp$, the component in the direction of $\mathrm{d}\boldsymbol{A}$, vanishes.) Therefore

$$\left\langle-\mathrm{div}\left[\left(\frac{\boldsymbol{u}^{\,2}}{2}+p\right)\boldsymbol{u}\right]\right\rangle_V = 0. \tag{4.3}$$

In a stationary situation the ∂_t-term on the left-hand side vanishes, too. The remaining, and thus necessarily also vanishing, contribution $\nu\langle\boldsymbol{u}\cdot(\Delta\boldsymbol{u})\rangle_V$ can be integrated by parts and thus be split into two mutually compensating terms, one representing the volume energy dissipation rate and the other the corresponding input rate of energy through the surface due to the viscous no-slip condition.

Write $\boldsymbol{u}\cdot\Delta\boldsymbol{u} = u_i\partial_j\partial_j u_i = \partial_j(u_i\partial_j u_i) - (\partial_j u_i)(\partial_j u_i)$ and symmetrize to find

$$\boldsymbol{u}\cdot\Delta\boldsymbol{u} = \partial_j(u_i(\partial_j u_i + \partial_i u_j)) - \tfrac{1}{2}(\partial_j u_i + \partial_i u_j)^2. \tag{4.4}$$

Incompressibility $\partial_j u_j = 0$ has been used. With the usual definition

$$\varepsilon = \frac{\nu}{2}\langle(\partial_i u_j + \partial_j u_i)^2\rangle_V, \tag{4.5}$$

for the balance with the viscous input from the surface we obtain

$$\varepsilon = \frac{\nu}{V}\oint \mathrm{d}A_j(u_i\partial_j u_i + u_i\partial_i u_j) = \frac{\nu}{V}\oint\mathrm{d}\boldsymbol{A}\cdot\left(\mathrm{grad}\frac{\boldsymbol{u}^2}{2} + (\boldsymbol{u}\cdot\nabla)\boldsymbol{u}\right). \tag{4.6}$$

In the limit of large aspect ratio Γ (or with periodic boundary conditions in the axial, z-direction) the V-surface consists of the two cylinder surfaces only. They contribute

I_1 plus I_2, the I being area averages of the integrand's r-component. For example,

$$I_2 = \frac{\nu A_2}{V}\left\langle \partial_r \frac{\boldsymbol{u}^2}{2} + ((\boldsymbol{u}\cdot\nabla)\boldsymbol{u})_r \right\rangle_{A_2} = \frac{2r_2\nu}{(r_2^2 - r_1^2)}\langle \ldots + \ldots \rangle_{A_2}.$$

The first term is $u_r\partial_r u_r + u_\varphi \partial_r u_\varphi + u_z \partial_r u_z = v_2 \partial_r r\omega\,|_2$. The second is (using (2.2)) $(\boldsymbol{u}\cdot\nabla)u_r - u_\varphi^2/r$. With (2.5) this gives $0 - v_2\omega_2$. Summing,

$$I_2 = \frac{2r_2\nu}{r_2^2 - r_1^2}\cdot r_2^2\omega_2\partial_r\langle\omega\rangle_2 = \frac{2}{r_2^2 - r_1^2}(-\omega_2 J^\omega).$$

The inner cylinder contributes correspondingly with another minus sign due to the area-normal pointing outwards. Together this results in

$$\varepsilon = \frac{2}{r_2^2 - r_1^2}(\omega_1 - \omega_2)J^\omega. \tag{4.7}$$

The laminar dissipation rate in particular, with J^ω_{lam} from (3.11), is calculated as

$$\varepsilon_{lam} = \nu\frac{r_1^2 r_2^2}{r_a^2}\left(\frac{\omega_1 - \omega_2}{d}\right)^2. \tag{4.8}$$

Along the line $\omega_1 = \omega_2$, i.e. for solid-body rotation, there is no laminar dissipation. Formulae (4.7) and (4.8) again emphasize the important role of the angular velocity ω in TC flow. The relevant transported quantity is ω and the relevant gradient for dissipation is $(\omega_1 - \omega_2)/d$. Since that can be positive as well as negative, ε_{lam} depends quadratically on the angular velocity gradient. Note that expression (4.7) – or the corresponding laminar one (4.8) – and the physical ansatz (4.1) are different. In the laminar case both differ by a factor of 2. As (4.7), (4.8) stem from the Navier–Stokes equations, we consider them to be the correct expressions for the dissipation rates.

We would like to mention that as an alternative to the decomposition (4.4) one could also have used the antisymmetric decomposition

$$\begin{aligned}\boldsymbol{u}\cdot\Delta\boldsymbol{u} &= \partial_j(u_i(\partial_j u_i - \partial_i u_j)) - \tfrac{1}{2}(\partial_j u_i - \partial_i u_j)^2 \\ &= \mathrm{div}(\boldsymbol{u}\mathrm{div}\boldsymbol{u}) + \mathrm{div}(\boldsymbol{u}\times\mathrm{curl}\boldsymbol{u}) - (\mathrm{div}\boldsymbol{u})^2 - (\mathrm{curl}\boldsymbol{u})^2.\end{aligned} \tag{4.9}$$

This identity would give rise to an alternative definition of a dissipation rate, namely

$$\hat{\varepsilon} \equiv \nu\langle(\mathrm{div}\boldsymbol{u})^2 + (\mathrm{curl}\boldsymbol{u})^2\rangle_V. \tag{4.10}$$

This also is a positive-definite expression and may thus serve as a dissipation rate. Its balance with the surface term is now

$$\hat{\varepsilon} = \frac{\nu}{V}\oint \mathrm{d}\boldsymbol{A}\cdot(\boldsymbol{u}\times\mathrm{curl}\boldsymbol{u} + \boldsymbol{u}\mathrm{div}\boldsymbol{u}).$$

The last term does not contribute, since $\mathrm{d}\boldsymbol{A}\cdot\boldsymbol{u} = 0$ at the cylinder surfaces. Calculating the first leads to

$$\hat{\varepsilon} = \frac{2}{r_2^2 - r_1^2}\left[(\omega_1 - \omega_2)J^\omega - 2\nu\,(\omega_1 L_1 - \omega_2 L_2)\right]. \tag{4.11}$$

For laminar TC flow we find

$$\hat{\varepsilon}_{lam} = \frac{\nu}{r_a^2}\left(\frac{L_2 - L_1}{d}\right)^2, \tag{4.12}$$

meaning that there is no dissipation of this type if $L_1 = L_2$. But constant angular momentum is different from constant angular velocity and does not correspond to

solid-body rotation $\omega(r) = \text{const}$. This physically unsatisfactory conclusion from the definition $\hat{\varepsilon}$ for the dissipation rate results in a physical preference for the symmetric definition (4.5) of the dissipation rate ε over $\hat{\varepsilon}$ from (4.10).

Note also that the symmetric dissipation rate (4.5) for incompressible flow can be reduced to the short form $\nu\langle(\partial_j u_i)^2\rangle_V$, if the additional term $\nu\partial_j u_i \partial_i u_j$ does not contribute. This happens for closed containers whose walls are at rest. It holds, e.g., for RB cells. The TC container is also closed, but the container walls rotate, $\boldsymbol{u}(r = r_1, r_2) \neq 0$. Therefore, this well-known short form for the dissipation rate cannot be used for TC flow.

Now, we are interested in the increase in the energy dissipation rate due to transverse convection between the cylinders beyond the circular laminar flow. Therefore, we introduce the 'convective' (or 'wind') dissipation rate per unit mass $\varepsilon_w \equiv \varepsilon - \varepsilon_{lam}$. Incidentally, the same excess dissipation rate would have been obtained from the dissipation rate $\hat{\varepsilon}$ defined via the curl-decomposition or antisymmetric dissipation definition: the additional terms in $\hat{\varepsilon}$ are expressed in terms of the control parameters only and therefore cancel with the subtraction of $\hat{\varepsilon}_{lam}$. We have

$$\varepsilon_w \equiv \varepsilon - \varepsilon_{lam} = \frac{2}{r_2^2 - r_1^2}(\omega_1 - \omega_2)\big(J^\omega - J^\omega_{lam}\big). \tag{4.13}$$

One can easily express ε_w in terms of the dimensionless angular velocity current, i.e. the angular velocity quasi-Nusselt number $N^\omega = J^\omega / J^\omega_{lam}$, and use (3.11) in the form $J^\omega_{lam} = \nu r_1^2 r_2^2 r_a^{-1}(\omega_1 - \omega_2)/d$ to obtain

$$\varepsilon_w = \nu r_1^2 r_2^2 r_a^{-2} \left(\frac{\omega_1 - \omega_2}{d}\right)^2 (N^\omega - 1). \tag{4.14}$$

This exact relation between the convective dissipation rate ε_w and the transverse ω-current quasi-Nusselt number N^ω clearly is the TC-analogue of the corresponding relation in thermal RB flow,

$$\varepsilon_w = \nu^3 L^{-4} Pr^{-2} Ra(Nu - 1), \tag{4.15}$$

which is at the heart of the scaling theory for RB (Grossmann & Lohse 2000, 2001, 2002; Grossmann & Lohse 2004). If we non-dimensionalize the convective dissipation rate ε in TC flow analogously, namely with $\nu^3 d^{-4}$ (corresponding to $\nu^3 L^{-4}$ in RB), we obtain from (4.14)

$$\frac{\varepsilon_w}{\nu^3 d^{-4}} \equiv \tilde{\varepsilon}_w = \sigma^{-2} \frac{d^2 r_a^2 (\omega_1 - \omega_2)^2}{\nu\kappa} (N^\omega - 1). \tag{4.16}$$

This suggests defining for TC flow a 'Taylor number' Ta † in close analogy to the Rayleigh number $Ra = \alpha_p g \Delta L^3/\nu\kappa$,

$$Ta = \frac{d^2 r_a^2 (\omega_1 - \omega_2)^2}{\nu\kappa} = \sigma \frac{d^2 r_a^2 (\omega_1 - \omega_2)^2}{\nu^2}. \tag{4.17}$$

There are several definitions of Taylor numbers in the literature; we prefer this one, which follows from the analogy with RB flow and makes (4.16) the same as (4.15). For the exact relations (4.14) or (4.16) between the non-dimensionalized dissipation

† There are slightly different definitions of a Taylor number in the literature. The notion was apparently first used by Chandrasekhar (1953). The Taylor number generally is defined $\propto \omega_1^2/\nu^2$, i.e. $\propto R_1^2$. But different length scales are used, e.g. d^4 instead of $r_1^2 d^2$, and usually no explicit η-dependence is included, as we do here, motivated by the analogy to Ra in RB flow.

rate $\tilde{\varepsilon} = \varepsilon/\nu^3 d^{-4}$ and the current N^ω we can now write

$$\tilde{\varepsilon}_w = \sigma^{-2}\, Ta\, (N^\omega - 1), \tag{4.18}$$

the perfect analogue of the corresponding RB relation (4.15).

Ta depends quadratically on the angular velocity gradient across the gap width. That seems to be in contrast to the linear dependence of Ra on the temperature difference between the bottom and the top plates in a Rayleigh–Bénard container. The simple explanation is that $(\omega_1 - \omega_2)^2$ is responsible for both the angular velocity difference $\omega_1 - \omega_2$ corresponding to the temperature difference Δ, and the driving centrifugal force, also $\propto \omega_1 - \omega_2$; the latter replaces the gravitational force g in the RB system. Since g has only one sign the temperature gradient can also only have one sign. We conclude that $(r_a^2/d)(\omega_1 - \omega_2)^2$ corresponds to the product $g \times \alpha_p \Delta$.

The Taylor number Ta is always positive, irrespective of co- or counter-rotation of the cylinders or if the inner or the outer cylinder is the faster one. When only the inner cylinder rotates and the outer cylinder is at rest, Ta is related to the inner-cylinder Reynolds number R_1 by

$$Ta = \sigma\, \frac{r_a^2}{r_1^2}\, R_1^2 = \frac{\sigma^2}{[(1+\eta)/2]^2} R_1^2. \tag{4.19}$$

Up to a geometrical factor, which often is near 1, Ta is the same as R_1^2.

5. Scaling of torque

5.1. *General considerations*

The discussion of the currents J and the convective dissipation rates ε_w has shown the very close analogy between TC and RB flow, even in fine details. But also differences have become obvious. For example, there is the factor of r^3 in the expression for the current with significant effects on the profile. Another characteristic TC feature is the control parameter $\sigma(\eta)$. It characterizes the geometry and enters through the boundary conditions, in contrast to the corresponding parameter in RB flow, the Prandtl number Pr, which is a fluid property and appears as a parameter in the equations of motion. But because of the close analogies in the physics of RB and TC flows, it might be possible to understand the torque scaling behaviour as a function of the rotational Reynolds numbers R_1, R_2, and η with similar arguments as used in thermal RB-convection to derive the Nusselt number scaling as a function of Ra and Pr. Apart from the formulae already derived in the previous sections, which are exact, we have to assume additional physical properties of TC flow in analogy to the corresponding ones in RB convection. Consequently, this section is more speculative than the previous ones and more input from experiment will be necessary in order to decide which assumption is right.

The following two ideas are assumed to be correct. First, we assume that the differences between the laminar and turbulent transport and dissipation are due to a velocity field which we call the wind and which we characterize by a typical amplitude U or Reynolds number $R_w = Ud/\nu$. The wind has, in particular, u_r- and u_z-components, which couple to u_φ via the Navier–Stokes and continuity equations. Thus the wind will also influence the u_φ-profile and vice versa. Component u_z has a boundary layer (BL), whose width δ is assumed to be connected to R_w by the classical Prandtl BL scaling (Prandtl 1905; Landau & Lifshitz 1987). According to Prandtl's argument the kinetic BL thickness scales as $\delta \sim \sqrt{\nu L/U}$, where L is the only available

length scale, namely the downstream length of the plate over which the wind U blows. The lateral extent is considered large (or even infinite). We argue that as long as there are remnants of the large-scale roll structures, the relevant length L is the gap width d between the cylinders, because this also sets the scale in the z-direction. The lateral extent is large if $2\pi r_i \gg d$. For the outer cylinder this means $1-\eta \ll 2\pi$, which can be considered as valid. For the inner cylinder the condition is less trivial, namely $\eta \gg 1/(2\pi+1) = 0.14$. Under these conditions the following formula is expected to describe the BL width of the transverse component u_z:

$$\frac{\delta}{d} = \frac{a}{\sqrt{R_w}}. \tag{5.1}$$

The parameter a is of order 1 and is determined by fitting to a data set. In RB flow we have found $a = 0.482$, cf. Grossmann & Lohse (2002). The inner and outer cylinder surfaces may require different prefactors a_1, a_2. The width δ is also a measure of the thickness of the u_r-component transition range between adjacent rolls. Owing to the conditions on η the following analysis is restricted to the range $1 > \eta \gg 0.14$, small or medium gap widths. This implies that σ is also restricted, $1 < \sigma \ll 5.4$.

If R_w becomes too small, δ becomes of the order of d, i.e. the wind boundary layer fills the entire gap. This happens if $R_w < (4a)^2 \approx 4$, because then $\delta_{max} \approx (d/4)$ (note that there are two boundary layers, namely near both rigid cylinder walls, the inner and the outer ones, each filling roughly half of $d/2$). For smaller R_w the width δ no longer scales with the wind amplitude but stays constant.

There is yet another proviso for the geometry. The wind (u_z, u_r) boundary layer covers the whole cylinder surfaces, which are curved. The application of Prandtl's BL scaling argument to a curved surface needs the proviso that its thickness δ must be much smaller than the radius of curvature of the curved surface. In our case this means $\delta \ll 2\pi r_1$, leading to the condition for applicability

$$\sqrt{R_w} \gg \frac{d\,a}{2\pi r_1} = a\,\frac{\eta^{-1}-1}{2\pi}.$$

This also signals that the limit of a very small inner cylinder, $\eta \to 0$, deserves particular care, because the formulae obtained then need corrections. For the smallest admissible value of $\eta \approx 0.14$, the right-hand side is close to 1, i.e. the condition of small enough δ is satisfied.

The second physical assumption is that in analogy to the thermal plumes in RB flow there are corresponding detachments from the boundary layers into the bulk, whose typical thickness should be λ, the ω-profile thickness. These objects might be hairpin vortices. They will be convected after detachment by the wind U. There is no *a priori* reason why λ should coincide with the wind boundary layer width δ, because λ measures the thickness of the BL of the longitudinal flow profile $\langle u_\varphi \rangle_{A,t}$, more precisely that of the profile $\langle \omega \rangle_{A,t}$, while δ characterizes the u_z-layer thickness. Experimental information on the difference between the u_φ- and the u_z-boundary layer thicknesses is highly desirable.

As discussed in § 3.1, there are in fact two ω-profile boundary layers, λ_1 and λ_2, which according to (3.10) are rather different unless η is near 1. To simplify the further discussion, we now introduce a mean ω-profile width λ. From (3.4) we have $J^\omega = \nu r_1^3 \partial\langle\omega\rangle_1/\partial(-r) = \nu r_2^3 \partial\langle\omega\rangle_2/\partial(-r)$. The inner and outer BL thicknesses are thus related by $r_1^3(\omega_1 - \bar{\omega})/\lambda_1 = r_2^3(\bar{\omega} - \omega_2)/\lambda_2$, with $\bar{\omega}$ the centre level of the ω-profile,

cf. (3.9). Adding the two J^ω expressions leads to

$$2N^\omega = \frac{\nu}{J^\omega_{lam}}\left[\frac{r_1^3}{\lambda_1}(\omega_1-\bar\omega)+\frac{r_2^3}{\lambda_2}(\bar\omega-\omega_2)\right]$$
$$= \sigma\left[\frac{r_1^3}{r_a^3}\frac{d}{\lambda_1}\frac{\omega_1-\bar\omega}{\omega_1-\omega_2}+\frac{r_2^3}{r_a^3}\frac{d}{\lambda_2}\frac{\bar\omega-\omega_2}{\omega_1-\omega_2}\right]. \tag{5.2}$$

This suggests introducing the following definition of a properly weighted average ω-width λ:

$$\frac{r_1^3}{\lambda_1}\approx\frac{r_2^3}{\lambda_2}\approx\frac{r_a^3}{\lambda}. \tag{5.3}$$

By this definition the $\omega_{1,2}$-dependence in (5.2) drops out and we have the relation

$$2\ N^\omega = \sigma\frac{d}{\lambda}, \tag{5.4}$$

which corresponds to the well-known RB flow relation for the thermal boundary layer thickness $\lambda_\theta/L = 1/(2Nu)$. Equations (5.4) and (5.1) connect the boundary layer thicknesses λ of the ω-profile and δ of the $u_{r,z}$ profiles with the quasi-Nusselt and the wind Reynolds numbers N^ω and R_w.

Besides the two prominent features of (i) the wind, characterized by the strength R_w and its BL thickness δ in the vicinity of the cylinder surfaces, and (ii) the existence of hairpin-like structures of thickness λ separating from the boundaries of the longitudinal component, there will be turbulent fluctuations in the flow between the rotating cylinders which we call background fluctuations.

To calculate next the torque in analogy to the Nusselt number we first consider the dimensionless dissipation rate $\tilde\varepsilon_w$. As in RB flow here we also decompose in the TC case the volume-averaged quantity ε_u into its bulk and its boundary layer contributions. We model the bulk dissipation by a term $\propto R_w^3$. This results from the stirring of the bulk fluid by the wind, whose energy U^2 is dissipated in the typical large-eddy turnover time d/U. This estimate for the dissipation is then non-dimensionalized by dividing through by $\nu^3 d^{-4}$, the chosen ε_w-unit.

The dissipation in the wind BL is modelled as

$$\nu\left(\frac{U}{\delta}\right)^2\frac{\delta}{d}\Big/\nu^3 d^{-4} = R_w^2\ \frac{d}{\delta},$$

if non-dimensionalized in the same way. The factor δ/d includes the weight of the BL relative to the bulk when averaging on r between r_1 and r_2. For the boundary layer width δ (5.1) is inserted, leading to a dissipation $\propto a^{-1}R_w^{5/2}$. Thus, together with (4.18), we have

$$\sigma^{-2}Ta(N^\omega-1) = c_1 a^{-1}\ R_w^{5/2} + \ c_2\ R_w^3. \tag{5.5}$$

The dimensionless constants c_1, c_2 have to be fitted to available data, as was done for RB flow in Grossmann & Lohse (2000, 2001, 2002). Physically, they represent some normalized correlation functions, which we consider as nearly independent of the control parameters ω_1, ω_2. A similar though simpler decomposition of the dissipation rate $\tilde\varepsilon_w$ (not considering geometry effects) has already been used in Eckhardt *et al.* (2000) and in van den Berg *et al.* (2003). Equation (5.5) reflects the varying weight of the boundary layer dissipation relative to that in the bulk. R_w is not yet known; it is part of the response of the system and will be determined together with the torque.

If R_w is too small, the factor δ/d stays constant in the range of smaller Reynolds numbers R_w (or R_1). The decomposition (5.5) then becomes

$$\tilde{\varepsilon}_w = c_1 R_w^2 + c_2 R_w^3, \quad R_w \text{ small } (< 4). \tag{5.6}$$

Next we revisit expression (3.13) for the dimensionless TC current N^ω of the angular velocity. It also is decomposed into two terms which scale differently. Inserting (3.11) and the σ-definition (3.12) we can write N^ω in the form

$$N^\omega = \sigma \left(\frac{r}{r_a}\right)^3 \frac{\langle u_r \omega\rangle_{A,t} - \nu \partial_r \langle\omega\rangle_{A,t}}{\nu(\omega_1 - \omega_2)/d}. \tag{5.7}$$

In the small-gap approximation the factor r^3/r_a^3 is about ≈ 1 and can be ignored, but in general it has to be taken into account. Except for the geometrical factors, the non-dimensionalized transverse angular velocity current N^ω consists of two terms. The first contains the correlation of the radial velocity u_r with ω, the other is the r-gradient of the $\langle\omega\rangle_{A,t}$ profile. In the first term we introduce $\tilde{\omega} = \omega/(\omega_1 - \omega_2)$ and $\tilde{u}_r = u_r/U$, where U is the amplitude of the wind. Note that one may also consider the amplitude u' of the u_r-fluctuations for U, if there is no large-scale coherent flow. In the second term we normalize ω in the same way. Both terms depend on the radial variable r, but the sum including the common prefactor $(r/r_a)^3$ is r-independent. We therefore can average over the gap width d:

$$N^\omega = \sigma R_w \left\langle \left(\frac{r}{r_a}\right)^3 \tilde{u_r}\tilde{\omega} \right\rangle_{V,t} - \sigma d \left\langle \left(\frac{r}{r_a}\right)^3 \partial_r \langle\tilde{\omega}\rangle_{A,t} \right\rangle_V. \tag{5.8}$$

The first contribution, besides the factor σR_w, is the properly non-dimensionalized and volume-weighted average of the u_r–ω correlation. The second one, besides σd, is the weighted profile slope. We estimate this as

$$\sigma\ d\ \left(\frac{r_1^3}{r_a^3}\frac{c_{3,1}}{\lambda_1} + \frac{r_2^3}{r_a^3}\frac{c_{3,2}}{\lambda_2}\right) = \sigma \frac{d}{\lambda} c_3, \quad \text{with } \ c_3 = c_{3,1} + c_{3,2}. \tag{5.9}$$

This transforms (5.8) into

$$N^\omega = \sigma \frac{d}{\lambda}\ c_3 + \sigma R_w c_4. \tag{5.10}$$

Both terms are r-independent but scale differently with R_w and thus with the control parameters. The dimensionless prefactors c_{3i} and c_4 might depend on η, since in particular the $\langle\omega\rangle$-slopes vary with the gap width individually. Details of the η dependence are not yet clear. But from analogy to RB flow we expect that the sum c_3 is nearly σ-independent. According to Prandtl's BL theory we assume that the thickness λ scales with the wind amplitude as

$$\frac{\lambda}{d} \propto \frac{1}{\sqrt{R_w}}. \tag{5.11}$$

In thermal convection across the boundary layer over a plate the factor of proportionality depends on the Prandtl number Pr; it is $\propto Pr^{-1/2}$ or $\propto Pr^{-1/3}$ depending on Pr being smaller or larger than 1, respectively, with an appropriate switch-over (Pohlhausen 1921; see also Grossmann & Lohse 2004). Also from Prandtl's BL theory we know that the field component u_y transverse to the plate scales in the same way with the longitudinal wind as the thickness of the longitudinal wind, namely as (5.1). We therefore use (5.11) without any further σ-dependence, by assumption. The remaining numerical prefactor is absorbed into c_3.

To emphasize the analogy between RB and TC we summarize all this with the following N^ω decomposition:

$$N^\omega = c_3\sigma\sqrt{R_w} + c_4\sigma R_w. \tag{5.12}$$

At least for small and medium gaps (η near 1) we expect that both c_3 and c_4 are practically independent of η as we found in RB flow. If η approaches the allowed small-η limit, the two boundary layer widths vary quite differently with η, which might result in a significant η-dependence of c_3. The constants c_3, c_4 together with c_1, c_2 are to be determined by comparison with experiment. Their possible dependence on the control parameters in this paper is assumed to be negligible.

Again, for decreasing R_w there is no longer any $\delta \propto d/\sqrt{R_w}$-scaling; the boundary layers fill the entire gap.

Note that in contrast to the partitioning of $\tilde{\varepsilon}_w$, which is based on the spatially different contributions to the dissipation in the BL and in the bulk, the decomposition of N^ω is defined by its scaling properties.

The case of counter-rotating cylinders deserves special attention. Here, a neutral surface between the inner and outer cylinders develops. Its location r_n is defined by the condition that the laminar profile has a zero, $v(r_n)=0$, and $r_1 \leqslant r_n \leqslant r_2$. This neutral surface separates and distinguishes between the inner part of the gap and the outer part. In the latter there is no direct structure formation. One expects an additional η- or σ-dependence beyond the explicit factors given already. As we know from the analysis of the stability line at the onset of vortex formation, cf. Esser & Grossmann (1996), the relevant gap for counter-rotating TC cylinders is no longer the geometric gap width $d=r_2-r_1$, but now the physically effective smaller gap $d_n=r_n-r_1$ between the neutral surface and the inner cylinder, at least for the onset of instability. Both r_n and d_n depend on η (or σ). We thus have to check carefully the decompositions (5.5) and (5.12) for counter-rotating TC flow. Further study is necessary for the torque scaling in the case of counter-rotating cylinders.

If all σ- or η-dependences are included, the two equations (5.5) and (5.12) are sufficient to calculate N^ω and R_w in terms of Ta and σ. Given N^ω one finds $G=\nu^{-2}J^\omega$ by multiplying N^ω with the laminar torque $\nu^{-2}J^\omega_{lam}$ from (3.11), all as functions of $\omega_1-\omega_2$.

In the often-met case of a stationary outer cylinder, $\omega_2=0$, cf. Lathrop *et al.* (1992*a*, *b*), Lewis & Swinney (1999) and Eckhardt *et al.* (2000, 2005), the control parameter is ω_1 or $R_1=r_1\omega_1 d/\nu$. The non-dimensionalized laminar torque is then

$$G_{lam} = \nu^{-2}J^\omega_{lam} = \frac{1}{\nu}r_1^2 r_2^2\frac{\omega_1}{r_a d} = \frac{\eta}{\frac{1}{2}(1+\eta)(1-\eta)^2}R_1, \tag{5.13}$$

and the physical torque is $G=G_{lam}\,N^\omega=\nu^{-2}\;J^\omega_{lam}\;N^\omega$, as is usual, see (3.14).

5.2. *Torque in small-gap TC flow*

Let us consider first the case of TC flow in a small gap between the cylinders. Then $\eta\approx 1$, $\sigma\approx 1$, and also $r/r_a\approx 1$. The relevant equations (5.5) and (5.12) for not too small N^ω then simplify to

$$Ta\;N^\omega = \;c_1\;a^{-1}R_w^{5/2} + \;c_2\;R_w^3, \tag{5.14}$$

$$N^\omega = \;c_3\sqrt{R_w} + \;c_4\;R_w. \tag{5.15}$$

If in both equations the boundary layer as well as the detached hairpin contributions dominate, having the smaller R_w-exponents, we obtain $Ta\,N^\omega \sim R_w^{5/2}$ and $N^\omega \sim \sqrt{R_w}$.

Then $Ta \sim R_w^2$ or $R_w \sim \sqrt{Ta} \sim R_1$ (using (4.19)) and $N^\omega \sim R_1^{1/2}$. Since the measured torque is $G = \nu^{-2}\ J_{lam}^{\omega}\ N^\omega$, the result for the torque and the wind in the boundary-layer-dominated range of small-gap TC flow is

$$G_{BL,BL} = \nu^{-2} J_{lam}^{\omega} N^\omega \sim R_1^{3/2} \quad \text{and} \quad R_w \sim R_1. \tag{5.16}$$

If, on the other hand, dissipation as well as current are dominated by the bulk or background fluctuations, the corresponding decomposition formulae are $Ta\ N^\omega \sim R_w^3$ and $N^\omega \sim R_w$. Thus, $R_w \sim \sqrt{Ta} \sim R_1$, the same as in the BL-BL case, and $N^\omega \sim R_1$. Consequently,

$$G_{bulk,bulk} = \nu^{-2} J_{lam}^{\omega} N^\omega \sim R_1^2 \quad \text{and} \quad R_w \ \sim \ R_1. \tag{5.17}$$

The scaling exponent α, defined by $G \propto R_1^\alpha$, in the two 'clean' cases of smaller R_1 with dominance of BL and hairpin contributions, or larger R_1 with dominance of bulk and background fluctuations, are thus 3/2 and 2. These values bound an interval that includes the measured exponents 1.65 to 1.80 in the range of R_1 from 10^4 to 10^6, see the introductory § 1. In this R_1-range one expects a gradual crossover from the $\sqrt{R_w}$ to the R_w dominance. Thus the limiting values 3/2 and 2 should be superimposed with varying weight. For example, 70% BL contribution and 30% bulk weight leads to $\alpha = 1.65$, while only 40% BL plus 60% bulk implies $\alpha = 1.80$. The agreement with the currently available data thus is satisfactory. In particular, it confirms and extends our previous ansatz in Eckhardt *et al.* (2000). As far as we are aware the arguments here and in Eckhardt *et al.* (2000) provide the first explanation of the experimentally found (cf. Lewis & Swinney 1999; Wendt 1933, etc.) continuous increase of α in the considered R_1-range: this increase is due to the decrease of the boundary- or detached-boundary-layer-dominated momentum transport in favour of the fluctuation-dominated one.

5.3. *Gap width effects*

We now include the expected dependence on the radius ratio η or gap width $1 - \eta$ and the corresponding $\sigma(\eta)$ (defined in (3.12)). We still consider co-rotating cylinders, because then no neutral surface develops. The decomposition formulae are the full ones, (5.5) and (5.12). We again start with the $\sqrt{R_w}$ case of BL and hairpin contributions for $\tilde{\varepsilon}_w$ as well as for N^ω. Then,

$$\sigma^{-2} Ta\ N^\omega \sim R_w^{5/2} \quad \text{and} \quad N^\omega \sim \sigma \sqrt{R_w}. \tag{5.18}$$

These two equations lead to $R_w \sim (Ta/\sigma)^{1/2}$ and $N^\omega \sim Ta^{1/4}\sigma^{3/4}$. The Taylor number Ta for a stationary outer cylinder $\omega_2 = 0$ is connected with the inner rotation Reynolds number R_1 by (4.19). Combining this gives

$$R_w \ \sim \ \frac{\sigma^{1/2}}{(1+\eta)/2} R_1. \tag{5.19}$$

In the $\eta \to 1$ case we recover $R_w \sim R_1$, cf. (5.16). The other finding is

$$N^\omega \ \sim \ \frac{\sigma^{5/4}}{\sqrt{(1+\eta)/2}} R_1^{1/2}. \tag{5.20}$$

Again, we regain the small-gap formula if $\eta \to 1$ and $\sigma(\eta) \to 1$.

The experimental dimensionless torque G from (3.14), and (5.13) is

$$G_{BL,BL} \propto \frac{((1+\eta)/2)^{7/2}}{\eta^{3/2}(1-\eta)^2}\ R_1^{3/2}. \tag{5.21}$$

η	0.95	0.9	0.8	0.7	0.6	0.5	0.4	0.3	0.2	0.1	0.05
$g_{bulk}(\eta)$	400	101	25.6	11.8	7.11	5.06	4.17	4.05	5.06	11.3	33.7

TABLE 2. The coefficient of the torque $G_{bulk,bulk}$, defined in (5.24) by $g_{bulk} = G_{bulk,bulk}/R_1^2 = [(1+\eta)/2]^4/(\eta^2(1-\eta)^2)$ versus the radius ratio η. Recall that for a large gap an additional η dependence is expected, i.e. $g_{bulk}(\eta)$ for η less than about 0.5 will change. The last two values for η are beyond the applicability of the present theory but are added to demonstrate the trend.

In terms of R_1 this torque increases strongly with $\eta \to 1$, i.e. for decreasing gap width. Note that $R_1 \propto d \propto (1-\eta)$, i.e. $G_{BL,BL}$ even increases for $\eta \to 1$ if it is considered as a function of the inner-cylinder rotation frequency ω_1, although more weakly, since $G_{BL,BL} \propto \omega_1^{3/2}/\sqrt{1-\eta}$. Thus the boundary-layer-determined torque $G_{BL,BL}$ will dominate in the smaller though turbulent R_1-ranges. In the limit of a very small gap this is the only relevant contribution to the torque G.

Next, we calculate the other 'clean' case of bulk and background fluctuation dominance, i.e. at larger R_1. The relevant equations are

$$\sigma^{-2}\, Ta\, N^{\omega} \;\sim\; R_w^3 \quad \text{and} \quad N^{\omega} \;\sim\; \sigma\, R_w. \tag{5.22}$$

From these one again obtains for the wind $R_w \propto \sqrt{Ta/\sigma}$ or

$$R_w \propto \frac{\sigma^{1/2}}{(1+\eta)/2}\, R_1. \tag{5.23}$$

The ω-transport current is different in its η-dependence, $N^{\omega} \sim \sigma R_w \sim \sigma\sqrt{Ta/\sigma} = \sqrt{\sigma\, Ta}$. Again using Ta from (4.19) and $\nu^{-2}J^{\omega}_{lam}$ from (5.13), we arrive at

$$G_{bulk,bulk} \;\sim\; \frac{[(1+\eta)/2]^4}{\eta^2(1-\eta)^2} R_1^2 \equiv g_{bulk}(\eta) R_1^2. \tag{5.24}$$

Since $R_1 \propto d \propto 1-\eta$, we see that $G_{bulk,bulk}$ remains finite for $\eta \to 1$ when considered as a function of ω_1 in the small-gap limit. This is expected, because for sufficiently narrow gap the ever-increasing boundary layer contribution must dominate the torque. The behaviour of $G_{bulk,bulk}/R_1^2 = g_{bulk}(\eta)$ as a function of η is given in table 2. We observe a rather strong dependence on η in the small-gap range $\eta \to 1$. Comparison with the experimental fit by Wendt (1933) seems promising: $\eta^{3/2}(1-\eta)^{-7/4}/g_{bulk}(\eta) = 0.46,\ 0.48,$ and 0.39 for the experimental radius ratios $\eta = 0.935$, 0.850, and 0.680, respectively.

According to (5.21), (5.24) and also according to Wendt (1933) the increase of G as η approaches 1 is somewhat stronger than found by Dubrulle & Hersant (2002), see their formulae (20)–(22). We shall come back to the η-dependence of the dimensionless current N^{ω} in figure 7.

We have to wait for more, and more precise, measurements to better check the theory. In particular, larger-gap data would be useful; in that case one can learn more about the possible additional dependence of the coefficients c_1, c_2, c_3, and c_4 on η. Also, the effects due to $\lambda \ll \delta$ will become stronger, see the next subsection.

5.4. *Scaling in large-gap TC flow*

In TC systems with a small gap and also for medium gap width the quasi-Prandtl number σ is near $\sigma \approx 1$. But σ increases considerably for large-gap systems, $\eta \to 0$, see table 1. Such an increase of the quasi-Prandtl number σ deserves attention, as we

know from Rayleigh–Bénard flow. For large Prandtl number the kinetic boundary layer, defined as the u-field BL of thickness λ_u, is much thicker than the thermal one and completely contains it. The width λ_θ of the thermal boundary layer is related to the Nusselt number by the relation $Nu = (L/2)/\lambda_\theta$. We remind the reader that our considerations are limited to $\eta > 0.14$, so that η cannot actually approach zero, but the trend for small η remains nevertheless.

Corresponding relations can be derived for the $\langle\omega\rangle_{A,t}$ profile BL thicknesses from (3.13) and (3.9),

$$N^\omega = \frac{r_1^3\Delta_1/\lambda_1}{2B} = \frac{r_2^3\Delta_2/\lambda_2}{2B}. \tag{5.25}$$

With $2B = r_1^2 r_2^2(\omega_1 - \omega_2)/r_a d$, cf. (3.11), we calculate

$$\lambda_1 = \frac{\Delta_1}{\omega_1 - \omega_2}\frac{r_1 r_a}{r_2^2}\frac{d}{N^\omega}, \quad \lambda_2 = \frac{\Delta_2}{\omega_1 - \omega_2}\frac{r_2 r_a}{r_1^2}\frac{d}{N^\omega}. \tag{5.26}$$

In the small-gap case this leads to the distance

$$\lambda = \frac{d/2}{N^\omega}, \tag{5.27}$$

in which the longitudinal angular velocity decreases or increases from its values at the cylinder surfaces to its flat bulk profile. λ is characteristic for the transport of the angular velocity ω, because it is defined in terms of N^ω. It should be compared with the width δ of the kinetic boundary layer, which according to (5.1) depends on $\sqrt{R_w}$. We thus distinguish between the boundary layer for the wind, which is supposed to be relevant for the large-scale circulation connected with u_r, u_z and which has the Prandtl width δ and, on the other hand, the transport boundary layer of width λ, which is relevant for the area-averaged profile of the longitudinal, azimuthal component, the angular velocity. This concept still requires experimental check and confirmation. In the following we investigate its consequences for the scaling of the torque for large-gap systems.

If the transport boundary layer width λ is less than the velocity boundary layer width δ, i.e. $\lambda/\delta = (1/2a)(\sqrt{R_w}/N^\omega) < 1$, this corresponds to the so-called 'upper' regime in thermal RB convection, realized for large Prandtl numbers (Grossmann & Lohse 2000, 2001, 2002; Grossmann & Lohse 2004). This upper regime should be distinguished from the 'lower' regime for small Prandtl numbers, in which the wind U reaches its full value within the thermal boundary layer, i.e. if $\delta < \lambda$. In the upper range, in contrast, the boundary layer of the transported quantity, i.e. θ in RB or ω in TC, has ended before the wind has reached its full amplitude U. Therefore, in the upper range U should be substituted by $U\lambda/\delta$ in the relevant expressions.

This physical argument seems to be transferable to TC flow. Then we expect that the angular velocity transport for larger σ, occurring for larger gap widths or smaller radius ratios η, will behave similarly to the upper range of RB convection. We analogously deal with this by adjusting the decomposition of N^ω according to (5.12) correspondingly. Instead of U (or R_w) we use $U\lambda/\delta$ (or $R_w\sqrt{R_w}/N^\omega$) and obtain

$$N^\omega = c_3\,\sigma\frac{R_w^{3/4}}{\sqrt{N^\omega}} + c_4\,\sigma\frac{R_w^{3/2}}{N^\omega}. \tag{5.28}$$

Then the upper-range scaling in the boundary-layer and hairpin-dominated case follows from $\sigma^{-2}TaN^\omega \sim R_w^{5/2}$ and $N^\omega \sim \sigma R_w^{3/4}/\sqrt{N^\omega}$. The latter relation is equivalent to $N^\omega \sim \sigma^{2/3}R_w^{1/2}$, i.e. up to a factor $\sigma^{1/3}$ we have the same wind scaling as before.

Together with the dissipation relation (5.14) this implies for the upper range (layer and hairpin dominated)

$$R_w \sim \sqrt{\frac{Ta}{\sigma^{4/3}}} \sim \frac{\sigma^{1/3}}{(1+\eta)/2}\ R_1 \quad \text{and} \quad N^\omega \sim \frac{\sigma^{5/6}}{\sqrt{(1+\eta)/2}}\ R_1^{1/2}. \tag{5.29}$$

In the upper range, where the BL set up by the velocities (u_z, u_r) is thicker than that set up by the ω-field, the G-exponent is $\alpha = 3/2$, as in the lower range.

If, on the other hand, the background fluctuations dominate, the starting equations are $\sigma^{-2} Ta N^\omega \sim R_w^3$ and $N^\omega \sim \sigma R_w^{3/2}/N^\omega$. Here, the latter expression leads to $N^\omega \sim \sigma^{1/2} R_w^{3/4}$. This relation between N^ω and R_w is different from $N^\omega \sim R_w$, valid in the lower regime treated before. The scaling solution for the contribution of the background fluctuations now is

$$R_w \sim \sigma^{-2/3} Ta^{4/9} \sim \frac{\sigma^{2/9}}{[(1+\eta)/2]^{8/9}}\ R_1^{8/9} \quad \text{and} \quad N^\omega \sim \frac{\sigma^{2/3}}{[(1+\eta)/2]^{2/3}}\ R_1^{2/3}, \tag{5.30}$$

leading with (5.13) to

$$G_{bulk,bulk} \sim \nu^{-2} J^\omega_{lam} N^\omega \sim \frac{(1+\eta)/2}{\eta^{1/3}(1-\eta)^2}\ R_1^{5/3}. \tag{5.31}$$

The exponent 5/3 is significantly smaller than 2 as derived above for the lower range, in which the $\langle\omega\rangle_{A,t}$ profile thickness exceeds the wind BL thickness, i.e. $\lambda > \delta$. We consider this a remarkable result which deserves experimental check. Its consequences will be discussed in detail in the next Section.

6. Comparison with experiment

The experiments referred to in § 1 were done with TC systems with η in a range where σ is still near to 1. Therefore, the results of §§ 5.1–5.3 (small gap width, 'lower case') might approximately describe them. For larger gap width, i.e. for smaller η, the quasi-Prandtl number σ increases ('upper case'). Then the G-exponent α is expected to lie between $\alpha = 3/2$ and $\alpha = 5/3$, according to (5.29) and (5.31). Since 5/3 is significantly smaller than 2, which we obtained in the lower regime, this implies that in the range of large R_1 we shall find, quite surprisingly, that with an increase of the gap width or a decrease of η, the exponent α will decrease from values near 2 towards values near 5/3.

Quantitatively, the crossover between the lower and upper ranges has been dealt with in Grossmann & Lohse (2000, 2001, 2002); Grossmann & Lohse (2004) by substituting for the full wind amplitude U in the N^ω decomposition (5.12) only the reduced wind amplitude $U\, g(\lambda/\delta)$ at the edge of the $\langle\omega\rangle_{A,t}$ profile. There, we have used the switching function

$$g(s) = \left(\frac{s^n}{1+s^n}\right)^{1/n} \quad \text{with} \quad s = \frac{\lambda}{\delta}. \tag{6.1}$$

The function g is 1 in the lower range $\lambda \gg \delta$, but reduces the wind to $U\lambda/\delta$ in the upper range with $\lambda \ll \delta$. In RB flow $n = 4$ has been used (Grossmann & Lohse (2000, 2001, 2002, 2004)), but there was not much difference with other values of n. The analysis in Eckhardt *et al.* (2000) indicated that there was a slight but noticeable difference in the scaling exponents from the pure bulk behaviour. We interpret this as an indication that the fluctuations in the current induce fluctuations in the boundary layer width and hence some averaging of the switching function (since the average

of a function usually does not equal the function of the average). We model this by allowing an additional algebraic scaling in the switching function, i.e.

$$g(s) = \frac{s^\gamma}{c_5 + s}, \tag{6.2}$$

where we expect γ to be near to one. The presence of the exponent $\gamma \neq 1$ also influences the asymptotic Reynolds number scaling. A repetition of the analysis of the preceeding section shows that in the boundary-layer-dominated region for small R_1, there is no effect. However, in the bulk-dominated regime, we find $R_w \sim R_1^{(4+4\gamma)/(5+4\gamma)}$ and $N^\omega \sim R_w^{(1+2\gamma)/(2+2\gamma)} \sim R_1^{(2+4\gamma)/(5+4\gamma)}$. For $\gamma = 1$, we recover the previous $N^\omega \sim R^{2/3}$ scaling. The numerical fit to the experimental data indicates that γ is slightly above one, so that the exponents for R_w and N^ω are somewhat larger, in agreement with previous findings Eckhardt *et al.* (2000).

The following decomposition, which replaces (5.12), describes both the lower and upper ranges as well as the crossover between them:

$$N^\omega = c_3\sigma\sqrt{R_w g(\lambda/\delta)} + c_4\sigma R_w g(\lambda/\delta). \tag{6.3}$$

Let us now compare the theory studied with experiment. To this end we need to determine the numerical coefficients $c_{1,2}$ and $c_{3,4}$ in the relevant expressions (5.14) and (5.15) for the lower and (5.14), (5.28) for the upper cases, in which $\delta < \lambda$ ('lower') or $\delta > \lambda$ ('upper'). This was done using the data of Lewis & Swinney (1999) by minimizing the relative error between the calculated and measured data. The data set contains a total of 571 pairs of torque G and Reynolds number R_1 of the inner cylinder, ranging between $R_1 = 2.98 \times 10^3$ and $R_1 = 8.76 \times 10^5$. Of these, the lowest values, up to $R_1 = 1.3 \times 10^4$ were excluded from the analysis to determine the c_i, since they are still dominated strongly by Taylor vortices, cf. Lathrop *et al.* (1992*b*) and Lewis & Swinney (1999). While they are not included in determining the parameters, they are shown with the experimental data in the figures below; typically, the omitted data points can be identified by their sharp deviation from the theoretical predictions. Omitting these points, 366 data pairs remain for fitting the parameters. The radius ratio is $\eta = 0.724$ and $\sigma = 1.0533$. To take the differences in the reference values for the dimensionless torque G into account, the values of Lewis & Swinney were divided by $\eta/[(1+\eta)/2)(1-\eta)^2] = 11.03$, see (5.13). As in the experiments, we only consider the case of a rotating inner cylinder and an outer cylinder at rest.

For the comparision, we use the relations between the current N^ω, the excess dissipation rate $\tilde{\epsilon}_w$ and the wind Reynolds number R_w, which according to (6.3) and (5.5) with (4.19) are

$$\frac{N^\omega}{\sigma} = c_3\sqrt{R_w g} + c_4 R_w g \tag{6.4}$$

and

$$\frac{1}{((1+\eta)/2)^2} R_1^2 N^\omega = c_1 a^{-1} R_w^{3/2} + c_2 R_w^3 . \tag{6.5}$$

The direct determination of N^ω for a prescribed R_1 leads to complicated implicit expressions. We therefore choose an alternative, analytically equivalent but numerically more convenient approach. Namely, we determine the Reynolds number R_1 from a prescribed current N^ω.

As a first step we calculate the wind Reynolds number R_w for given N^ω from (6.4). This requires the switching function g from (6.2). It describes the transition between the lower and upper regimes, where $s = \lambda/\delta$ is much larger or much smaller than one,

respectively. The value of g depends on the ratio s of the boundary layer widths. We assume that it depends on σ or η only through its arguments λ and δ. From the definition of the variable $s = \lambda/\delta = \sigma a^{-1}\sqrt{R_w}/(2\,N^\omega)$ we conclude

$$R_w = (2a\ N^\omega \sigma^{-1} s)^2. \tag{6.6}$$

Introducing this expression for R_w into (6.4) one notes that it is just the combination $\hat{N}^\omega \equiv N^\omega/\sigma$ which appears, leading to

$$\hat{N}^\omega = c_3(2a\hat{N}^\omega)\ s\sqrt{g(s)} + c_4(2a\hat{N}^\omega)^2\ (s^2 g(s)). \tag{6.7}$$

This is a quadratic equation for the auxiliary quantity ϕ defined as $\phi(s) \equiv (s\sqrt{g(s)})^2$, i.e. equation (6.4) for the current $\hat{N}^\omega$ becomes

$$\hat{N}^\omega = c_3(2a\hat{N}^\omega)\sqrt{\phi} + c_4(2a\hat{N}^\omega)^2\phi. \tag{6.8}$$

For a given value of the current $\hat{N}^\omega$, this equation can be solved for ϕ. The value of s corresponding to this ϕ can then be determined from the functional form of g, (6.2), and the definition of ϕ:

$$\phi = s^2 g(s) = \frac{s^{2+\gamma}}{c_5 + s}\,. \tag{6.9}$$

This allows one to determine s numerically from the just calculated ϕ. Knowing s and taking again the current $\hat{N}^\omega$, we can obtain the wind Reynolds number R_w from (6.6).

The second step is the direct evaluation of R_1 for prescribed N^ω together with the just calculated R_w from the dissipation equation (6.5). These two steps thus give R_1 versus N^ω, provided the coefficients c_i are already known.

In order to determine the optimal parameter values c_i, we proceed in the same manner. For the experimentally measured currents N^ω we calculate corresponding Reynolds numbers R_1' as just described with preliminary values c_i' of the parameters. We then adjust the parameters by least-square optimization such that $(R_1' - R_1)/R_1$ becomes minimal. For the least-square optimization c_i of the parameters c_i' we note that as long as the scale of the wind Reynolds number R_w is not yet set by measurement, one of the coefficients can be absorbed in R_w, cf. Grossmann & Lohse (2002). We choose to keep $c_2 = 29.3$ fixed.

Our least-mean-square fit to the relative $(R_1' - R_1)$-differences resulted in the parameters $c_1 = 0.435$, $c_2 = 29.3$, $c_3 = 0.220$, $c_4 = 0.0147$, $c_5 = 1.99 \times 10^{-6}$ and $\gamma = 1.23$. The errors in the Reynolds number range included are less than about 1%.

We begin our comparison between observations and theory with the familiar log–log plots of G versus R_1 in figure 1. On such a plot, the data, the previously given log-law fit, and the variable-exponent power-law curves of the upper and lower ranges fall essentially on top of each other.

For better resolution we have introduced in Grossmann & Lohse (2000, 2001, 2002); Grossmann & Lohse (2004) reduced linear–log plots, in which the relevant quantity is divided by some power law with an arbitrary, but nearby and fixed exponent. Since we expect a torque scaling with exponents between 1.5 and 2, we show in figure 2 the results for a torque normalized by $R^{1.75}$, intermediate between the two exponents. In this figure we also include a comparison to the expression

$$G = K_7 \frac{\eta^2}{(1-\eta)^{3/2}} \frac{R_1^2}{\left(\ln\left(\eta^2(1-\eta)R_1^2/K_8\right)\right)^{3/2}} \tag{6.10}$$

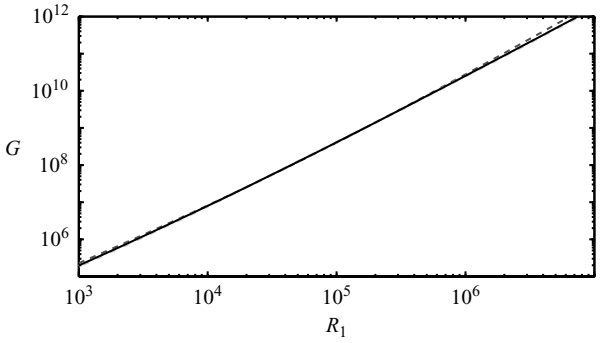

FIGURE 1. Log–log plots of G versus R_1 for the data from Lewis & Swinney (1999). The circles are the data points. The continuous line is derived from the present theory, and the lighter dash-dotted line from a fit to a logarithmic profile (the two curves are indistinguishable in this graph). The dashed line represents the fit to the lower range case $\lambda > \delta$.

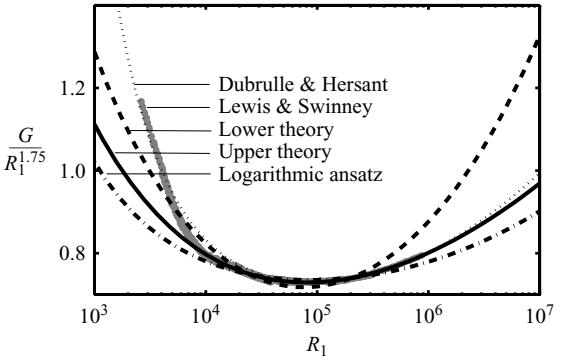

FIGURE 2. The torque G divided by $R_1^{1.75}$ versus R_1 in a linear–log presentation. The exponent 1.75 has been chosen as the mean value in the relevant range $1.5 < \alpha < 2$. Compared to figure 1 deviations between the different curves are now visible. The grey dots are the data from Lewis & Swinney (1999). The current theory for the lower range is indicated by a dashed line, the one for the upper range theory with a full line. The optimal fit with a logarithmic variation is indicated by the dash-dotted line, the results from Dubrulle & Hersant (2002) by the dotted line. We used the improved coefficients, as explained below (6.10). For R_1 below about 10^4 the data are strongly influenced by the still present spatially coherent flow patterns and depend on the number of rolls and on aspect ratio Γ (cf. Lewis & Swinney 1999), while the theory applies for turbulent TC advection without long ranging spatial correlations. This is visible in the systematic deviation between the data and the theoretical curves for R_1 below 10^4.

given by Dubrulle & Hersant (2002).† To obtain the good agreement in the reduced representation shown in the figure, we had to determine the constants again and improve their values from $K_7 = 0.5$ and $K_8 = 10^4$ to $K_7 = 0.484$ and $K_8 = 0.699 \times 10^4$, respectively.

The quality of the fit can be assessed from the pointwise relative error shown in figure 3. Both the logarithmic profile and the present decomposition argument reproduce the variations in the experimental data to better than 1%.

† In Dubrulle & Hersant (2002) the exponent in the denominator was shown inside the argument of the logarithm, but it should be outside. We thank B. Dubrulle for pointing this out.

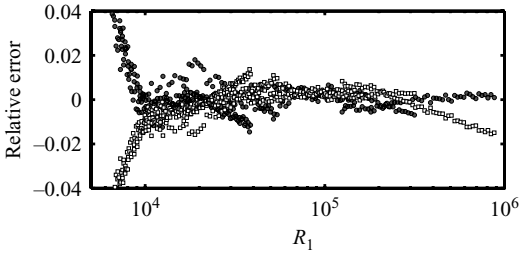

FIGURE 3. The relative error of the upper-range power-law fit with variable exponent and of the log-law fit. The power law (black dots) presents the data within about 1%, as does the log-law (open squares).

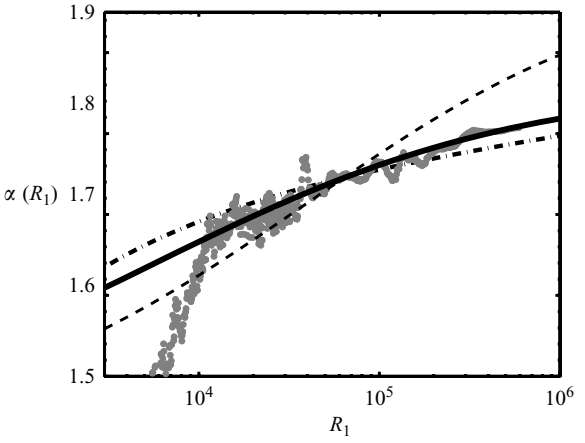

FIGURE 4. The scaling exponents $\alpha(R_1)$. The lower-range and upper-range exponents are shown as dashed and solid lines respectively. For larger R_1 they either approach the value $\alpha = 2$ or bend down again towards the asymptotic value $\alpha = 5/3$. The exponent corresponding to the log-law (dash-dotted) lies above that of the upper and lower regime for R_1 below about 10^5. For larger values the order of the local slopes reverses. The asymptotic values discussed in §§ 5.2 and 5.4 are reached for much larger Reynolds numbers only.

The above analysis shows that the data can be represented quite well by a power law with varying exponent $\alpha(R_1)$, expressing the varying fraction of the contributions of the boundary layers and of the bulk to the current J and the dissipation rate of the wind ε_w. In previous work (cf. Lathrop *et al.* 1992*a*, *b*; Lewis & Swinney 1999) the exponents of the local power-law fits to their data have been plotted. The local exponents for the present theory are shown in figure 4.

For completeness, we also consider $2\pi G(R_1)/R_1^2 \equiv f(R_1)$, figure 5, which in pipe flow is the expression for the skin friction factor. Here, too, the modelling of the data as a superposition of scaling laws performs well.

An essential feature of the theory is the wind Reynolds number R_w, which characterizes the transverse velocity fluctuations. Its absolute scale remains unkown until it is determined by measurement. However, its dependence on the Reynolds number R_1, externally imposed by the boundary conditions, can be studied. It is shown in figure 6. Consistent with the observations in Eckhardt *et al.* (2000) it decays with increasing Reynolds number.

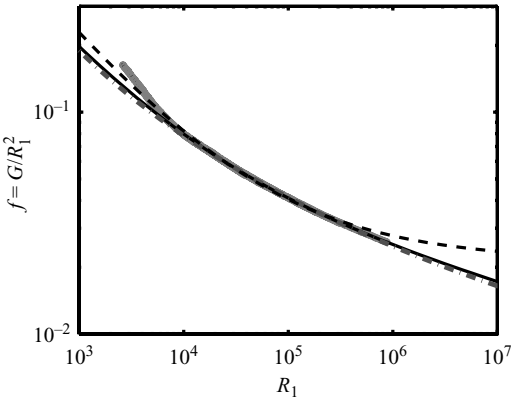

FIGURE 5. Friction factor $f(R_1) = G(R_1)/R_1^2$. Curves have the same meaning as in figure 2. Note the good agreement in the range of the data, the upper range case being superior for large R_1.

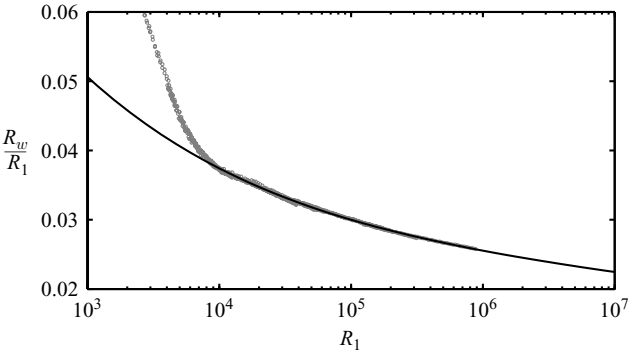

FIGURE 6. The Reynolds number R_w of the amplitude $U = \nu L^{-1} R_w$, describing the order of magnitude of the transverse component u_r, u_z of the velocity field $\boldsymbol{u}$, which is responsible for the convective transport of the longitudinal component $u_\varphi/r = \omega$. To show how R_w differs from the external control parameter R_1 the ratio R_w/R_1 is plotted. The full line is the theoretical interpolation for the upper case theory, the circles are the values corresponding to the experimental data. In the upper case the wind ratio R_w/R_1 decreases asymtotically to zero. R_w itself increases with the control parameter R_1 as $R_w \approx 0.085 R_1^{0.94}$. The exponent also is variable: 0.94 indicates its mean value in the relevant range. The experimental data appear twice, since the two different models give two different representations of the data. In the lower case (not shown) R_w approaches R_1 for large R_1, up to a factor. (No meaningful comparison with the log-law can be given, as its derivation does not contain the concept of a wind.)

We conclude the comparison to experimental data by testing the variations with η. We assume, in analogy to the calculations in RB flow, that none of the parameters, the coefficients c_1, c_2, c_3, c_4, and c_5 nor the exponent γ, depend on σ. Then from the now known c_i one can calculate the current N^ω, the torque $G = \nu^{-2} J^\omega_{lam}\, N^\omega$, and the wind Reynolds number R_w for any other experiment with given σ or η as functions of R_1 in the range of interest by using (6.4) and (6.5). In particular, on introducing a rescaled Reynolds number

$$\hat{R}_1 \equiv \frac{\sqrt{\sigma}}{(1+\eta)/2} R_1 \tag{6.11}$$

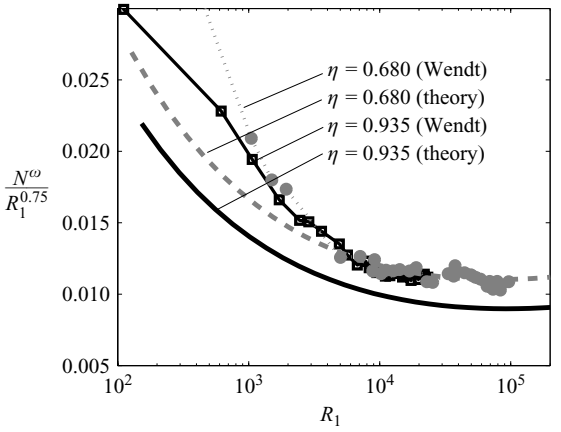

FIGURE 7. Rescaled angular momentum current $N^\omega/R_1^{3/4}$ vs. Reynolds number R_1 for different radius ratios η and the results from Wendt (1933). The full lines and squares are theory and experiment for $\eta = 0.935$, and the dashed lines and circles for $\eta = 0.680$, respectively.

the equations for the current (6.4) and the dissipation (6.5) take the form $\hat{N}^\omega = \ldots$ and $\hat{R}_1^2\hat{N}^\omega = \ldots$, where the $\ldots$ denote the right-hand sides which are independent of η. Therefore, for a given pair of $\hat{N}^\omega$ and $\hat{R}_1$, we can find the values for a value η by mapping

$$(\hat{R}_1, \hat{N}^\omega) \to \left(\frac{(1+\eta)/2}{\sqrt{\sigma}}\hat{R}_1, \sigma\hat{N}^\omega\right). \tag{6.12}$$

This mapping implies that a pair of $(\hat{R}_1, \hat{N}^\omega)$ values moves towards smaller R_1 and larger N^ω as η decreases from 1. Taking the R_1-dependence of N^ω into account, the differences are not too large, less than about 20% for $R_1 \approx 10^5$. It is for this reason that Wendt (1933) could show in his figure 12 an approximate data collapse. The current predictions and a few representative points from Wendt (1933) are shown in figure 7. It would be useful to have data with an accuracy that could test the predictions better.

7. Summary and conclusions

In summary, we have derived an exact analogy between TC and RB flow, which in contrast to earlier analogies even holds in turbulent regimes. The role of the Nusselt number in RB flow is taken by N^ω, the flux of the angular velocity current $J^\omega = r^3[\langle u_r\omega\rangle_{A,t} - \nu\partial_r\langle\omega\rangle_{A,t}]$, made dimensionless by its laminar value. The role of the Rayleigh number is taken by the Taylor number $Ta = (d^2r_a^2(\omega_1-\omega_2)^2)/(\nu\kappa)$ and the role of the Prandtl number is taken by a 'geometric' Prandtl number $\sigma = (((1+\eta)/2)/\sqrt{\eta})^4$. Then the dimensionless convective energy dissipation rate (i.e. the excess above the laminar case) can be written as $\tilde{\varepsilon}_w = \sigma^{-2}\,Ta\,(N^\omega - 1)$, in perfect analogy to the RB case. In the laminar case the transport of J^ω from the inner to the outer cylinder occurs through diffusion; in the turbulent case it is through the 'wind of turbulence' (in the TC context the turbulent remnants of the laminar 'Taylor vortices'), just as in the RB case for the heat.

We then extended Grossmann & Lohse's (2000, 2001, 2002, 2004) unifying RB scaling theory to the TC case. Though the results are encouraging (§ 6), we should stress the difficulties of this extension.

(i) From our point of view one main difficulty originates from the stronger interdependence of the BL thicknesses δ (of the wind velocity) and λ (of the angular velocity) compared to the RB case, where at least in the passive scalar limit the kinetic BL thickness is independent of the thermal BL thickness.

(ii) Another complication is that the top–bottom symmetry in RB flow cannot be replaced by an inner- vs. outer-cylinder symmetry, owing to radius-dependent weight factors. This introduces an extra free parameter into the theory.

(iii) Next, while in thermal RB convection the currently known experiments cover wide ranges in the (Ra, Pr)-phase space which very clearly belong to either the lower range case with $\delta \ll \lambda$ or the upper range case with $\delta \gg \lambda$, cf. Grossmann & Lohse (2000, 2001, 2002); Grossmann & Lohse (2004), the quasi-Prandtl number σ is close to unity or slightly larger than $\sigma \approx 1$ for the currently available data. Therefore, the fluctuations of the velocity field $\boldsymbol{u}$ will lead to fluctuating values of the thickness ratio $s = \lambda/\delta$. The longitudinal BL width λ and the transversal wind BL width δ thus will also fluctuate, i.e. there may be frequent switching between the lower and the upper cases.

(iv) Finally, the data on $Nu(Ra, Pr)$ and $Re(Ra, Pr)$ obtained in recent high-precision RB experiments are of much higher quality than the corresponding TC data, both regarding the precision and the covered parameter range. There are many intrinsic problems in obtaining TC data of analogous quality, namely handling TC cells with two rotating cylinders, measurements inside the rotating system, friction, exploring large radii ratios, etc., and it will be very challenging to overcome all these problems.

The success of the scaling theory presented here can only be evaluated once more data on torque and the velocity field between the cylinders, of high precision and covering a wider range of parameters, become available. Altogether there are many experimental challenges in verifying or improving the various details of the torque analysis presented for TC flow, including the various profiles and the boundary layer widths.

The authors thank Dan Lathrop for stimulating discussions and Harry Swinney for providing the data from Lewis & Swinney (1999). They would like to acknowledge – in addition to their Universities – the kind hospitality of the Lorentz Center, Leiden (The Netherlands) and of the University of Maryland through its Burgers Programme (BE). This work was supported through grants by the Deutsche Forschungsgemeinschaft DFG, is part of the FOM research program, financially supported by NWO, and was further supported by the European Union EU under contract HPRN-CT-2000-00162.

REFERENCES

van den Berg, T. H., Doering, C., Lohse, D. & Lathrop, D. 2003 Smooth and rough boundaries in turbulent Taylor–Couette flow. *Phys. Rev.* E **68**, 036307.

Bradshaw, P. 1969 The analogy between streamline curvature and buoyancy in turbulent shear flow. *J. Fluid Mech.* **36**, 177–191.

Breuer, M., Wessling, S., Schmalzl, J. & Hansen, U. 2004 Effect of inertia in Rayleigh–Bénard convection. *Phys. Rev.* E **69**, 026302.

Chandrasekhar, S. 1953 The instability of a layer of fluid heated from below and subject to Coriolis forces. *Proc. R. Soc. Lond.* A **217**, 306–327.

Doering, C. R. & Constantin, P. 1992 Energy-dissipation in shear driven turbulence. *Phys. Rev. Lett.* **69**, 1648–1651.

Dubrulle, B. & Hersant, F. 2002 Momentum transport and torque scaling in Taylor–Couette flow from an analogy with turbulent convection. *Eur. Phys. J.* B **26**, 379–386.

Eckhardt, B., Grossmann, S. & Lohse, D. 2000 Scaling of global momentum transport in Taylor–Couette and pipe flow. *Eur. Phys. J.* B **18**, 541–544.

Eckhardt, B., Grossmann, S. & Lohse, D. 2005 Energy and dissipation balances in rotating flows. In *Progress in Turbulence* (ed. J. Peinke, A. Kittel, S. Barth & M. Oberlack), pp. 47–50. Springer.

Eckhardt, B., Grossmann, S. & Lohse, D. 2007 Fluxes and energy dissipation in thermal convection and shear flows. *Europhys. Lett.* **78**, 24001.

Esser, A. & Grossmann, S. 1996 Analytic expression for Taylor–Couette stability boundary. *Phys. Fluids* **8**, 1814–1819.

Funfschilling, D. & Ahlers, G. 2004 Plume motion and large scale circulation in a cylindrical Rayleigh–Bénard cell. *Phys. Rev. Lett.* **92**, 194502

Grossmann, S. & Lohse, D. 2000 Scaling in thermal convection: A unifying view. *J. Fluid. Mech.* **407**, 27–56.

Grossmann, S. & Lohse, D. 2001 Thermal convection for large Prandtl number. *Phys. Rev. Lett.* **86**, 3316–3319.

Grossmann, S. & Lohse, D. 2002 Prandtl and Rayleigh number dependence of the Reynolds number in turbulent thermal convection. *Phys. Rev.* E **66**, 016305.

Grossmann, S. & Lohse, D. 2004 Fluctuations in turbulent Rayleigh–Bénard convection: The role of plumes. *Phys. Fluids* **16**, 4462–4472.

Landau, L. D. & Lifshitz, E. M. 1987 *Fluid Mechanics*. Pergamon.

Lathrop, D. P. 1992 Turbulent drag and transport in high Reynolds number flow. PhD thesis, University of Texas at Austin.

Lathrop, D. P., Fineberg, J. & Swinney, H. S. 1992*a* Turbulent flow between concentric rotating cylinders at large Reynolds numbers. *Phys. Rev. Lett.* **68**, 1515–1518.

Lathrop, D. P., Fineberg, J. & Swinney, H. S. 1992*b* Transition to shear-driven turbulence in Couette-Taylor flow. *Phys. Rev.* A **46**, 6390–6405.

Lewis, G. S. & Swinney, H. L. 1999 Velocity structure functions, scaling, and transitions in high-Reynolds-number Couette-Taylor flow. *Phys. Rev.* E **59**, 5457–5467.

Lim, T. T. & Tan, K. S. 2004 A note on power-law scaling in a Taylor–Couette flow. *Phys. Fluids* **16**, 140–144, erratum *Phys. Fluids* **16**, 2712.

Marcus, P. S. 1984 Simulation of Taylor–Couette flow. Part 1. Numerical methods and comparison with experiment. *J. Fluid Mech.* **146**, 45–64.

Marcus, P. S. 1984 Simulation of Taylor–Couette flow. Part 2. Numerical results for wave-vortex flow with one travelling wave. *J. Fluid Mech.* **146**, 65–113.

Nickerson, E. C. 1969 Upper bounds on the torque in cylindrical Couette flow. *J. Fluid Mech.* **38**, 807–815.

Pohlhausen, E. 1921 Der Wärmeaustausch zwischen Festkörpern und Flüssigkeiten mit kleiner Reibung und kleiner Wärmeleitung. *Z. Angew. Math. Mech.* **1**, 115–121.

Prandtl, L. 1905 Über Flüssigkeitsbewegung bei sehr kleiner Reibung. In *Verhandlungen des III. Int. Math. Kongr., Heidelberg 1904*, pp. 484–491. Leipzig: Teubner.

Smith, G. P. & Townsend, A. A. 1982 Turbulent Couette flow between concentric cylinders at large Taylor numbers. *J. Fluid Mech.* **123**, 187–217.

Taylor, G. I. 1936*a* Fluid friction between rotating cylinders. I. Torque measurements. *Proc. R. Soc. Lond.* A **157**, 546–564.

Taylor, G. I. 1936*b* Fluid friction between rotating cylinders. II. Distribution of velocity between concentric cylinders when outer one is rotating and inner one is at rest. *Proc. R. Soc. Lond.* A **157**, 565–578.

Tong, P., Goldburg, W. I., Huang, J. S. & Witten, T. A. 1990 Anisotropy in turbulent drag reduction. *Phys. Rev. Lett.* **65**, 2780–2783.

Wendt, F. 1933 Turbulente Strömungen zwischen zwei rotierenden Zylindern. *Ing. Arch.* **4**, 577–595.